NAVAL POSTGRADUATE SCHOOL
Monterey, California

THESIS

EFFECTS OF WELDING ON ENERGY DISSIPATION IN A WATERTIGHT BULKHEAD

by

Jon S. Erskine

June 2003

Thesis Advisor: Young Shin
Co-Advisor: Ilbae Ham

Approved for public release, distribution is unlimited.

THIS PAGE INTENTIONALLY LEFT BLANK

REPORT DOCUMENTATION PAGE			Form Approved OMB No. 0704-0188
Public reporting burden for this collection of information is estimated to average 1 hour per response, including the time for reviewing instruction, searching existing data sources, gathering and maintaining the data needed, and completing and reviewing the collection of information. Send comments regarding this burden estimate or any other aspect of this collection of information, including suggestions for reducing this burden, to Washington headquarters Services, Directorate for Information Operations and Reports, 1215 Jefferson Davis Highway, Suite 1204, Arlington, VA 22202-4302, and to the Office of Management and Budget, Paperwork Reduction Project (0704-0188) Washington DC 20503.			
1. AGENCY USE ONLY ***(Leave blank)***	**2. REPORT DATE** June 2003	**3. REPORT TYPE AND DATES COVERED** Master's Thesis	
4. TITLE AND SUBTITLE: Effects of Welding on Energy Dissipation in a Watertight Bulkhead			**5. FUNDING NUMBERS**
6. AUTHOR(S) Jon S. Erskine			
7. PERFORMING ORGANIZATION NAME(S) AND ADDRESS(ES) Naval Postgraduate School Monterey, CA 93943-5000			**8. PERFORMING ORGANIZATION REPORT NUMBER**
9. SPONSORING /MONITORING AGENCY NAME(S) AND ADDRESS(ES) N/A			**10. SPONSORING/MONITORING AGENCY REPORT NUMBER**
11. SUPPLEMENTARY NOTES The views expressed in this thesis are those of the author and do not reflect the official policy or position of the Department of Defense or the U.S. Government.			
12a. DISTRIBUTION / AVAILABILITY STATEMENT Approved for public release, distribution is unlimited.			**12b. DISTRIBUTION CODE**

13. ABSTRACT ***(maximum 200 words)***

Surface combatants face a wide range of threats and perhaps the most destructive of these is the underwater explosion generated by a mine or a torpedo. The shock wave generated by an underwater explosion can cause severe damage or even a catastrophic failure. As the shock wave hits the ship, its energy is transmitted through the structural members of the ship. The purpose of this thesis is to examine how this energy is transmitted through the watertight bulkhead of a DDG and how the welded stiffeners affect the bulkhead's energy damping properties. To investigate the effects of the welding, the bulkhead was modeled both as a finite element model and as a scaled physical model. The modes and natural frequencies of the bulkhead were first calculated using PATRAN and NASTRAN. Using a one half scale model, the bulkhead was excited using random noise over a 250 Hz frequency span while measuring the accelerations at 60 points along the panel. These measured accelerations were then used to calculate the frequency response of the bulkhead and the damping ratios as a function of frequency. By plotting the damping ratios versus frequency for each measurement point on the bulkhead, there can be a better understanding of how energy waves propagate through a welded structure.

14. SUBJECT TERMS Damping, Rayleigh Damping, Weldment Effects, Modal Analysis, Complex Exponential Method			**15. NUMBER OF PAGES** 81
			16. PRICE CODE
17. SECURITY CLASSIFICATION OF REPORT Unclassified	**18. SECURITY CLASSIFICATION OF THIS PAGE** Unclassified	**19. SECURITY CLASSIFICATION OF ABSTRACT** Unclassified	**20. LIMITATION OF ABSTRACT** UL

NSN 7540-01-280-5500 Standard Form 298 (Rev. 2-89)
Prescribed by ANSI Std. 239-18

THIS PAGE INTENTIONALLY LEFT BLANK

Approved for public release, distribution is unlimited.

EFFECTS OF WELDING ON ENERGY DISSIPATION IN A WATERTIGHT BULKHEAD

Jon S. Erskine
Ensign, United States Navy
B.S. Naval Architecture, US Naval Academy, 2002

Submitted in partial fulfillment of the
requirements for the degree of

MASTER OF SCIENCE IN MECHANICAL ENGINEERING

from the

NAVAL POSTGRADUATE SCHOOL
June 2003

Author: Jon S. Erskine

Approved by: Young Shin
Thesis Advisor

Ilbae Ham
Co-Advisor

Young Kwon
Chairman, Department of Mechanical Engineering

THIS PAGE INTENTIONALLY LEFT BLANK

ABSTRACT

Surface combatants face a wide range of threats and perhaps the most destructive of these is the underwater explosion generated by a mine or a torpedo. The shock wave generated by an underwater explosion can cause severe damage or even a catastrophic failure. As the shock wave hits the ship, its energy is transmitted through the structural members of the ship. The purpose of this thesis is to examine how this energy is transmitted through the watertight bulkhead of a DDG and how the welded stiffeners affect the bulkhead's energy damping properties. To investigate the effects of the welding, the bulkhead was modeled both as a finite element model and as a scaled physical model. The modes and natural frequencies of the bulkhead were first calculated using PATRAN and NASTRAN. Using a one half scale model, the bulkhead was excited using random noise over a 250 Hz frequency span while measuring the accelerations at 60 points along the panel. These measured accelerations were then used to calculate the frequency response of the bulkhead and the damping ratios as a function of frequency. By plotting the damping ratios versus frequency for each measurement point on the bulkhead, there can be a better understanding of how energy waves propagate through a welded structure.

THIS PAGE INTENTIONALLY LEFT BLANK

TABLE OF CONTENTS

THIS PAGE INTENTIONALLY LEFT BLANK

LIST OF FIGURES

LIST OF TABLES

THIS PAGE INTENTIONALLY LEFT BLANK

ACKNOWLEDGMENTS

I would like to extend my sincerest thanks to my thesis advisor Professor Young Shin and co-advisor Professor Ilbae Ham. Professor Shin's vast knowledge in the field of vibrations, his insights, and his continual support and encouragement throughout the year has made this thesis possible. Special thanks to Professor Ilbae Ham whose patience, efforts, ability to clearly explain the complexities involved in vibrations and damping, and his kindness will never be forgotten and without whom this thesis would not have been possible.

I would also like to thank my office mate, thesis partner, advisor on all things Navy, and my friend LT Charles "Chuck" Ehnes. Without his help throughout this past year with classes and thesis work alike this year would have been next to impossible and as I head to the fleet I will keep in mind his words of advice.

Additional thanks to Tom Christian and Sheila Deiotte whose tireless efforts to setup and modify the Virtual Instrument software are deeply appreciated.

Finally I would like to thank my family who has supported me at every step of the way. Your love and support has kept me going through the good times and especially when the light at the end of the tunnel seemed almost out of sight. I love you all very much.

THIS PAGE INTENTIONALLY LEFT BLANK

I. INTRODUCTION

A. BACKGROUND

Naval surface combatants face a wide range of threats from the air, the surface and below the surface of the ocean. One of the most destructive and perhaps most probable threats comes from underwater explosions generated by detonating torpedoes or mines. The underwater explosions generated by these weapons create shock waves that race out towards a ship at nearly five thousand feet per second. When the shock wave reaches the hull of a ship, some of the energy is reflected back into the water but more importantly, some of that energy is transmitted to the ship and its structural members. As this energy travels through the ship it causes structures to oscillate or vibrate over a range frequencies. Vibrations occurring at resonant frequencies can result in large amplitude displacements which can cause severe damage or even catastrophic failures which is important to understand their effects on a ship's critical systems and structures.

Of key concern to the Navy is how a ship and its individual components can dissipate the energy imparted by the shock wave of an underwater explosion. This dissipation of energy (either over time or distance) is known as damping. The ability of a structure to dissipate energy can be affected by many things but primarily by friction at structural joints. [1] Construction of Navy ships today relies heavily upon welding, as such, understanding the effects welded members have on a structure's ability to dissipate energy is of critical importance.

In a system such as a steel watertight bulkhead it is clear that the damping is related to the material properties but it has also been hypothesized that stress concentrations present in the system will have an affect on the overall damping. According to Betts, Bishop, and Price, the stress concentrations "account for large local increases in the alternating field stress…thereby contributing markedly higher damping than the surrounding material that is subject only to the field stress."[2] Additionally they hypothesize that fatigue cycling will cause a build up of "exceptionally high local damping."[2] In the watertight bulkhead, the stress concentrations are the result of the shrinkage that occurs in the area around the welded stiffeners. The shrinkage induces tensile yield stress parallel to the weld. The area of these residual stresses has been

shown to extend between 4½ to 6 plate thicknesses either side of the weld line which can account for approximately 15% of the plate material, meaning that the overall damping of the panel is increased.[2]

In a test performed by Betts, Bishop, and Price a mild steel bar, clamped at the ends, and held in tension in a Denison machine, was subjected to flexural symmetric vibrations (of small amplitude). The damping of the panel was measured by an analysis of the decay of free vibration recorded by an accelerometer attached to the center of the bar. Plotting the loss coefficient versus mean stress showed that the mean stress appears to be a "relevant parameter in deciding the level of damping"[2] and that "damping is significantly increased in the presence of a mean tensile yield stress." As a result of their experiment, the authors believed that "welding effects, together with stress concentrations, are among the most important sources of hull damping in deformation modes."[2]

B. OBJECTIVES

The objectives of this research are to investigate what effect welding has on a beam stiffened watertight bulkhead in a DDG. In particular the purposes of this research are to determine if the presence of welds in a structure increase the overall damping of the structure, does the damping ratio increase at the measurement point as the number of welds between the measurement location and the excitation source increases, and to compare the Rayleigh damping coefficients from experimental data to those estimated from ship shock trial data.

C. TEST SPECIMEN DESCRIPTION

This investigation was specifically targeted at the damping characteristics of the watertight bulkhead in a Flight IA Arleigh Burke Destroyer. Specimen 1 was a rectangular steel panel (102" x 18" x 0.25") made of A-36 steel, without any welds or stiffeners. The unwelded panel was used to gather baseline damping data, how does the damping ratio change in relation to distance from the excitation source. Specimen 2 was constructed to be a scale model of the watertight bulkhead. Using the structural drawings

provided by NAVSEA, a one half scale model (9’ x 4’) made of A-36 steel, was created using 9 gauge steel plating, 11 gauge transverse stiffeners, and 12 gauge vertical stiffeners. The following tables and figures give the dimensions and characteristics of each specimen.

SPECIMEN 1 – UNWELDED PANEL

Table 1.1 Dimensions of Unwelded Panel

A-36 Steel	
Length	102 in
Width	18 in
Thickness	0.25 in

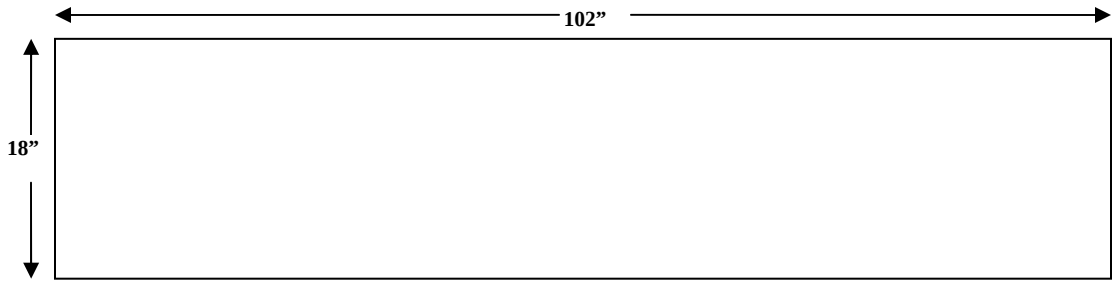

Figure 1.1 Drawing of Unwelded Panel

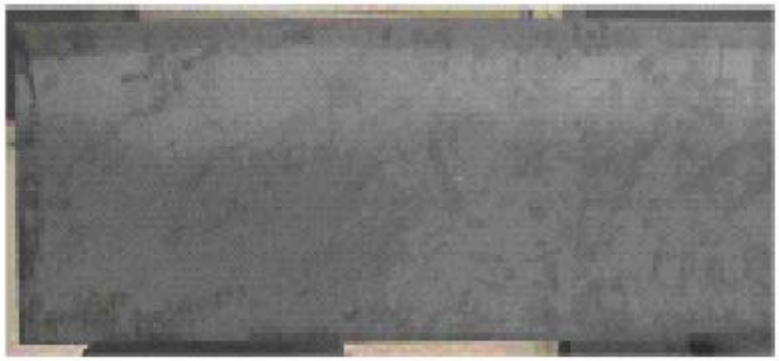

Figure 1.2 Picture of Unwelded Panel

SPECIMEN 2 – WELDED WATERTIGHT BULKHEAD

Table 1.2 Dimensions of Watertight Bulkhead

A-36 Steel	
PLATE	
Length	9 ft
Width	4 ft
Thickness	9 Gauge
VERTICAL STIFFENERS	
Length	47.6875 in
Width	2.5 in
Thickness	12 Gauge
HORIZONTAL STIFFENERS	
Length	9 ft
Width	2.5 in
Thickness	11 Gauge

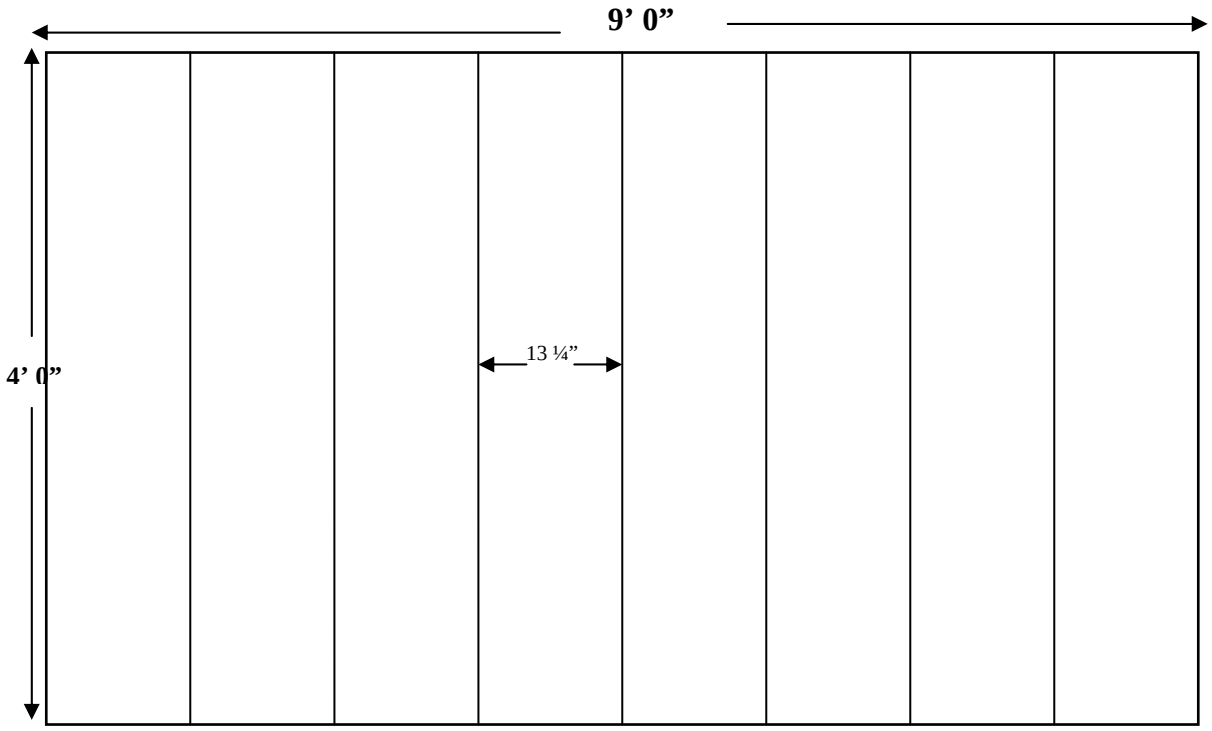

Figure 1.3 Drawing of Watertight Bulkhead

Figure 1.4 Picture of Watertight Bulkhead

THIS PAGE INTENTIONALLY LEFT BLANK

II. THEORY

A. ASSUMPTIONS

When a system such as a ship or a particular component of a ship is excited by an external force, it will respond by vibrating and will continue to do so until the force is no longer applied. Once the exciting force stops, the system will over time return to its static (non-moving) state. The ability of a structure to dissipate the input energy over a period of time or across the body of the structure itself is a phenomenon known as damping.

Total damping in a system can be the combination of many different types of damping, including viscous damping, structural damping, and Coulomb damping. Although in real structures, many of these forms of damping may be present, a fairly accurate mathematical model of the damping can be created assuming only viscous damping is present. Assuming viscous damping makes calculating the damping properties of the system more convenient equations than if structural or Coulomb damping were considered, while at the same time still providing good approximations of the true total damping.

Viscous damping is "the dissipation of energy that occurs when a particle in a vibrating system is resisted by a force that has a magnitude proportional to the magnitude of the velocity of the particle and direction opposite to the direction of the particle."[3] Viscous damping can be expressed by the following equation

$$F_d = c\dot{x} \tag{2.1}$$

c = constant of proportionality

Another key assumption in creating a mathematical model of the damping that can be conveniently calculated is to assume that the system experiences linear proportional damping. In other words, the damping of the system is linearly proportional to the mass and the stiffness of the system. For a multi-degree-of-freedom system such as a ship or watertight bulkhead, these assumptions lead to the following damping equation;

$$[C] = \alpha[M] + \beta[K] \tag{2.2}$$

These assumptions form the basis for the model by which the damping values across the watertight bulkhead will be calculated.

B. BASIC DAMPING THEORY

A vibratory system such as a ship or a watertight bulkhead comprises "means for storing potential energy (spring), means for storing kinetic energy (mass or inertia) and means by which the energy is gradually lost (damper)."[3] The governing equation of motion for a damped single degree of freedom (SDOF) system experiencing free vibration is:

$$m\ddot{x} + c\dot{x} + kx = F(t) \tag{2.3}$$

where

m = Mass constant

c = Damping constant

k = Stiffness constant

The homogenous solution to the differential equation of motion, Equation (2.1) is found by assuming $x = e^{st}$ and $F(t) = 0$. Substituting into the differential equation yields;

$$\left(ms^2 + cs + k\right)e^{st} = 0 \tag{2.4}$$

is satisfied for all values of t when

$$s^2 + \frac{c}{m}s + \frac{k}{m} = 0 \tag{2.5}$$

Known as the characteristic equation, equation (2.5) has two roots:

$$s_{1,2} = -\frac{c}{2m} \pm \sqrt{\left(\frac{c}{2m}\right)^2 - \frac{k}{m}} \tag{2.6}$$

The general solution of the differential equation is thus given by;

$$x = Ae^{s_1 t} + Be^{s_2 t} \tag{2.7}$$

where A and B are constants evaluated from the initial conditions of displacement and velocity at time zero; x(0) and $\dot{x}(0)$. Substituting (2.6) into (2.7)

$$x = e^{-(c/2m)t}\left(Ae^{\left(\sqrt{(c/2m)^2 - k/m}\right)t} + Be^{-\left(\sqrt{(c/2m)^2 - k/m}\right)t} \right) \tag{2.8}$$

The value of the damping term $(c/2m)^2$ determines the energy dissipation properties of the system. If the damping term is more than (*k/m*), then the exponents in (2.8) are real numbers and no oscillations will occur, a case known as overdamped. If the damping term is less than (*k/m*), the exponent becomes an imaginary number, $\pm i\sqrt{k/m-(c/2m)^2}\,t$, and results in oscillations that will diminish exponentially with time, a case known as underdamped. For most real structures, the damping ration is almost always less than 10 percent and is therefore underdamped, thus the mathematical models for this thesis are also assumed to the underdamped case. Finally, if the damping term is equal to (*k/m*) and the radical is equal to zero. This case is known as critical damping, c_c

$$c_c = 2m\sqrt{\frac{k}{m}} = 2m\omega_n = 2\sqrt{km} \tag{2.9}$$

As a result any damping can be expressed in terms of the critical damping by a nondimensional number ζ, the damping ratio, where $\zeta = \frac{c}{c_c}$. Hence equation (2.6) becomes

$$s_{1,2} = \left(-\zeta \pm \sqrt{\zeta^2 - 1}\right)\omega_n \tag{2.10}$$

and the differential equation of motion can now be expressed by[4]

$$\ddot{x} + 2\zeta\omega_n\dot{x} + \omega_n^2 = \frac{1}{m}F(t) \tag{2.11}$$

C. FREQUENCY RESPONSE FUNCTION

The purpose of this thesis is to find the damping ratio of the watertight bulkhead as a function of time. In order to calculate the damping ratios a modal analysis will be performed, but in order to perform the analysis it is first necessary to determine how the structure will respond to an input stimulus. For the modal analysis it is more convenient to express the equation of motion, equation (2.3) in the frequency rather than time domain. The transformation is easily performed using a Fourier transform of the equation of motion in the time domain. The resulting equation of motion in the frequency domain is given by

$$[-m\omega^2 + jc\omega + k]X(\omega) = F(\omega) \tag{2.12}$$

or

$$X(\omega) = H(\omega)F(\omega) \tag{2.13}$$

where

$$H(\omega) = \frac{1}{-m\omega^2 + jc\omega + k} = \frac{1}{k}\frac{1}{1-(\omega/\omega_n)^2 + i2\zeta(\omega/\omega_n)} \tag{2.14}$$

and

$$\omega_n^2 = \frac{k}{m} \qquad\qquad \zeta = \frac{c}{c_c} = \frac{c}{2\sqrt{km}} \tag{2.15}$$

ω_n = Natural Frequency

ζ = Damping Ratio

c_c = Critical damping coefficient

From Equation 2.3 it can be seen that the response of the system $\{X(\omega)\}$, is directly related to the system forcing function $\{F(\omega)\}$, by $\{H(\omega)\}$. If the forcing function and the response are known, then $\{H(\omega)\}$ known as the Frequency Response Function (FRF) can be simply calculated by:

$$H(\omega) = \frac{X(\omega)}{F(\omega)} \tag{2.16}$$

The roots of the characteristic equation, Equation (2.5) are complex roots even though the FRF is a function of a real-valued independent variable ω. These complex roots are also known as the modal frequencies. Rewriting the FRF as a function of the modal frequencies gives:

$$H(\omega) = \frac{1/m}{(j\omega - \lambda_1)(j\omega - \lambda_1^*)} \tag{2.17}$$

where

$\lambda_1 = -\omega_1\zeta_1 + j\omega_1\sqrt{1-\zeta_1^2}$

A partial fraction expansion of the FRF leads to:

$$H(\omega) = \frac{A}{(j\omega - \lambda_1)} + \frac{A^*}{(j\omega - \lambda_1^*)} \tag{2.18}$$

The A term and its complex conjugate A^* represent the modal constant or mode shapes of the structure.

The above FRF is valid for a system with a single degree of freedom, for more complex systems with N degrees of freedom (NDOF) requires the governing equation of motion to be described using the mass, stiffness, and damping matrices.

$$[M]\{\ddot{x}\}+[C]\{\dot{x}\}+[K]\{x\}=\{F(t)\} \tag{2.19}$$

The individual FRF's for the NDOF system is developed in the same way as the FRF for the SDOF system and the overall FRF is constructed by linear superposition, resulting in:

$$H_{pq}(\omega)=\sum_{r=1}^{n}\frac{A_{pqr}}{(j\omega-\lambda_r)}+\frac{A_{pqr}^*}{(j\omega-\lambda_r^*)} \tag{2.20}$$

where

ω = Frequency Variable

p = Measured Degree-of-freedom (Response)

q = Measured Degree-of-freedom (Input)

r = Modal Vector Number

A_{pqr} = Residue

λ_r = System Pole

n = Number of Modal Frequencies

D. MODAL ANALYSIS

Modal analysis is "the process of determining the modal parameters (natural frequencies, damping factors, modal vectors, and modal scaling) of a linear, time-invariant system." [3] In order to perform an experimental modal analysis on a structure, four basic assumptions are made:[3]

1. *The structure is assumed to be linear.*
   The response of the structure to any combination of forces, simultaneously applied, is the sum of the individual responses to each of the forces acting alone.

2. *The structure is time invariant.*
   The parameters that are to be determined are constants.

3. *The structure obeys Maxwell's reciprocity.*

A force applied at a degree-of-freedom *p* causes a response at degree-of-freedom *q* that is the same as the response at degree-of-freedom *p* caused by the same force applied at degree-of-freedom *q*.

4. *The structure is observable.*
   The input-output measurements that are made contain enough information to generate and adequate behavioral model of the structure.

The first step in understanding how the modal parameters of a system are extracted is to understand the response of a single degree-of-freedom system to a disturbance. By calculating the response function for a system, its characteristics or modal parameters can be calculated for any given input.

E. EXTRACTION OF MODAL PARAMETERS [1][5]

One method used to extract the modal parameters of the system is the Complex Exponential Method (CEM). The CEM requires the use of the time domain version of the system response which is found by taking the Inverse Fourier Transform of the FRF or the Receptance (displacement/force) $\alpha(\omega)$ of a viscously damped system.

$$H(\omega) = \alpha(\omega) = \sum_{r=1}^{n} \frac{A_r}{(j\omega - \lambda_r)} + \frac{A_r^*}{(j\omega - \lambda_r^*)} = \sum_{r=1}^{2N} \frac{A_r}{j\omega - \lambda_r} \tag{2.21}$$

The corresponding Impulse Response Function in the time domain is given by:

$$h(t) = \sum_{r=1}^{2N} A_r e^{\lambda_r t} \tag{2.22}$$

Additionally, the Mobility (velocity/force) $Y(\omega)$ of the system can be related to the Receptance:

$$Y(\omega) = j\omega\alpha(\omega) \tag{2.23}$$

The velocity form of the IRF is expressed as:

$$\dot{h}(t) = \sum_{r=1}^{2N} A_r \lambda_r e^{\lambda_r t} \tag{2.24}$$

From the velocity form of the IRF, the sampled velocity data set can be expressed as follows:

$$\dot{h}_0, \dot{h}_1, \dot{h}_2, ..., \dot{h}_q = \dot{h}(0), \dot{h}(\Delta t), \dot{h}(2\Delta t), ..., \dot{h}(q\Delta t) \tag{2.25}$$

To simplify the following equations, let:

$$e^{\lambda_r \Delta t} \rightarrow V_r \tag{2.26}$$

Thus the j-th sample data of Equation (2.14) is expressed as:

$$\dot{h}_j = \dot{h}(j\Delta t) = \sum_{r=1}^{2N} A_r \lambda_r V_r (j\Delta t) = \sum_{r=1}^{2N} A_r \lambda_r V_r \tag{2.27}$$

If extended to the full data set of q sample data, Equation (2.17) becomes;

$$\begin{aligned}
\dot{h}_0 &= \lambda_1 A_1 + \lambda_2 A_2 + \cdots + \lambda_{2N} A_{2N} \\
\dot{h}_1 &= V_1 \lambda_1 A_1 + V_2 \lambda_2 A_2 + \cdots + V_{2N} \lambda_{2N} A_{2N} \\
\dot{h}_2 &= V_1^2 \lambda_1 A_1 + V_2^2 \lambda_2 A_2 + \cdots + V_{2N}^2 \lambda_{2N} A_{2N} \\
&\vdots \quad\quad \vdots \quad\quad\quad \vdots \quad\quad\quad\quad \vdots \\
\dot{h}_q &= V_1^q \lambda_1 A_1 + V_2^q \lambda_2 A_2 + \cdots + V_{2N}^q \lambda_{2N} A_{2N}
\end{aligned} \tag{2.28}$$

Provided that the number of sample points q exceeds 4N, the above equation can be used to set up an eigenvalue problem, the solution of which yields the complex natural frequencies contained in the parameters V_1, V_2, etc.

Multiplying each equation in (2.18) by the coefficient β_j yields the following equations

$$\begin{aligned}
\beta_0 \dot{h}_0 &= \beta_0 A_1 + \beta_0 A_2 + \cdots + \beta_0 A_{2N} \\
\beta_1 \dot{h}_1 &= \beta_1 V_1 A_1 + \beta_1 V_2 A_2 + \cdots + \beta_1 V_{2N} A_{2N} \\
\beta_2 \dot{h}_2 &= \beta_2 V_1^2 A_1 + \beta_2 V_2^2 A_2 + \cdots + \beta_2 V_{2N}^2 A_{2N} \\
&\vdots \quad\quad\quad \vdots \quad\quad\quad\quad \vdots \quad\quad\quad\quad\quad \vdots \\
\beta_q \dot{h}_q &= \beta_q V_1^q A_1 + \beta_q V_2^q A_2 + \cdots + \beta_q V_{2N}^q A_{2N}
\end{aligned} \tag{2.29}$$

Summing the equations in (2.19) results in;

$$\sum_{i=0}^{q} \beta_i \dot{h}_i = \sum_{j=1}^{2N} (A_j \sum_{i=0}^{q} \beta_i V_j^i) \tag{2.30}$$

The coefficients β_j are taken as the coefficients in the equation;

$$\beta_0 + \beta_1 V + \beta_2 V^2 + \beta_3 V^3 + \cdots + \beta_q V^q = 0 \tag{2.31}$$

With roots V_1, V_2, ⋯, V_q.

By finding the values of the β coefficients, the roots of the system, and hence the natural frequencies, can be determined. Recalling that q is the number of data points from the IRF and 2N is the number of degrees-of-freedom of the system's model, by setting q=2N;

$$\sum_{j=0}^{2N} \beta_i V_r^j = 0\,; \qquad \text{r = 1,2N} \tag{2.32}$$

This makes the right hand side terms of (2.20) equal to zero and (2.22) can be restated as;

$$\sum_{i=0}^{2N-1} \beta_i \dot{h}_i = -\dot{h}_{2N} \qquad \text{by setting } \beta_{2N} = 1 \tag{2.33}$$

By repeating these steps using different IRF data points and choosing new data sets that overlap with the first set for all but one item, leads to a full set of 2N equations:

$$\begin{bmatrix} \dot{h}_0 & \dot{h}_1 & \dot{h}_2 & \cdots & \dot{h}_{2N-1} \\ \dot{h}_1 & \dot{h}_2 & \dot{h}_3 & \cdots & \dot{h}_{2N} \\ \vdots & \vdots & \vdots & \vdots & \vdots \\ \dot{h}_{2N-1} & \dot{h}_{2N} & \dot{h}_{2N+1} & \cdots & \dot{h}_{4N-2} \end{bmatrix} \begin{Bmatrix} \beta_0 \\ \beta_1 \\ \vdots \\ \beta_{2N-1} \end{Bmatrix} = - \begin{Bmatrix} \dot{h}_{2N} \\ \dot{h}_{2N+1} \\ \vdots \\ \dot{h}_{4N-1} \end{Bmatrix} \tag{2.34}$$

or

$$\left[\dot{h}\right]_{2Nx2N} \{\beta\}_{2Nx1} = -\left\{\tilde{h}\right\}_{2Nx1} \tag{2.35}$$

The unknown coefficients β can be found from (2.24) and the roots from equation (2.21), thus the natural frequencies can be found using the following relationship;

$$V_r = e^{\lambda_r \Delta t} \tag{2.36}$$

Finally by using equation (2.18) the corresponding modal constants A_1, A_2,$\cdots$, A_{2N} can be calculated and written as;

$$\begin{bmatrix} 1 & 1 & 1 & \cdots & 1 \\ V_1 & V_2 & V_3 & \cdots & V_{2N} \\ V_1^2 & V_2^2 & V_3^2 & \cdots & V_{2N}^2 \\ \vdots & \vdots & \vdots & \cdots & \vdots \\ V_1^{2N-1} & V_2^{2N-1} & V_3^{2N-1} & \cdots & V_{2N}^{2N-1} \end{bmatrix} \begin{Bmatrix} A_1\lambda_1 \\ A_2\lambda_2 \\ A_3\lambda_3 \\ \vdots \\ A_{2N}\lambda_{2N} \end{Bmatrix} = \begin{Bmatrix} \dot{h}_0 \\ \dot{h}_1 \\ \dot{h}_2 \\ \vdots \\ \dot{h}_{2N-1} \end{Bmatrix} \tag{2.37}$$

or

$$[V]\{A\} = \{h\} \tag{2.38}$$

To verify the modal parameters calculated using the above Complex Exponential Method, the originally measured time histories are compared to the synthesized or regenerated time histories. From equations (2.11), (2.12), and (2.13)

$$\hat{Y}(\omega) = \sum_{r=1}^{N} \frac{j\omega A_r}{j\omega - \lambda_r} + \frac{j\omega A_r^*}{j\omega - \lambda_r^*}; \qquad \lambda_r = -\omega_r \zeta_r + j\omega_r \sqrt{1-\zeta_r^2} \tag{2.39}$$

or

$$\hat{Y}(\omega) = \sum_{r=1}^{2N} \frac{j\omega A_r}{j\omega - \lambda_r}; \qquad \lambda_r \Rightarrow \lambda_r^*, \;\; A_r \Rightarrow A_r^*, \text{ for r > N} \tag{2.40}$$

F. RAYLEIGH DAMPING[1]

When analyzing multiple degree-of-freedom systems it is important to consider the effect of damping on the complex frequencies and modal vectors. Although one or a combination of the aforementioned damping cases may be present in a particular structure, it is again more convenient to consider damping that is linearly proportional to the system mass and stiffness matrices. This case of damping is known as proportional or Rayleigh damping case and has been characterized by the following equation:

$$[C] = \alpha [M] + \beta [K] \tag{2.41}$$

Performing a coordinate transformation to diagonalize the system mass and stiffness matrices also diagonalizes the system damping matrix.

Applying the mass normalized modal matrix $[\varphi]$ to equation (2.31) yields;

$$[\varphi]^T [C][\varphi] = [2\omega_r \zeta_r]_{diag} = \alpha I + \beta \left[\omega_r^2\right]_{diag} \tag{2.42}$$

Using equation (2.32) for all 2N modes

$$\begin{aligned} \alpha + \beta\omega_1^2 &= 2\omega 1\zeta_1 \\ \alpha + \beta\omega_2^2 &= 2\omega 1\zeta_2 \\ &\vdots \\ \alpha + \beta\omega_{2N}^2 &= 2\omega 1\zeta_{2N} \end{aligned} \tag{2.43}$$

or

$$[W]_{2Nx2} \begin{Bmatrix} \alpha \\ \beta \end{Bmatrix} = \{Z\}_{2Nx1} \tag{2.44}$$

Finally the parameters α and β from equation (2.34) are calculated by matrix pseudo-inverse;

$$\begin{Bmatrix} \alpha \\ \beta \end{Bmatrix} = \left([W]_{2x2N}^T [W_{2x2N}] \right)^{-1} [W]_{2x2N}^T \{Z\}_{2Nx1} \tag{2.45}$$

G. HALF-POWER POINT METHOD[4]

Another method for calculating the damping ratio in a system is known as the Half-Power Point method. The first step is to record the frequency response function of the system in response to an excitation force. For each response peak, the value Q is a measure of the sharpness of the peak. When a resonant frequency is reached, $\omega/\omega_n = 1$ and the amplitude peak is given by;

$$x_{res} = \frac{F_0/k}{2\zeta} \tag{2.46}$$

The "half-power points" are defined as the points located on either side of resonance where x=0.707x_{max}. Letting x=0.707x_{max} and squaring the expression for frequency response amplitude yields;

$$\frac{1}{2}\left(\frac{1}{2\zeta}\right)^2 = \frac{1}{\left[1-\left(\frac{\omega}{\omega_n}\right)^2\right]^2 + \left[2\zeta\left(\frac{\omega}{\omega_n}\right)\right]^2} \tag{2.47}$$

Solving for $(\omega/\omega_n)^2$;

$$\left(\frac{\omega}{\omega_n}\right)^2 = \left(1-2\zeta^2\right) \pm 2\zeta\sqrt{1-\zeta^2} \tag{2.48}$$

Assuming ζ ≪ 1 and neglecting higher order terms;

$$\left(\frac{\omega}{\omega_n}\right)^2 = 1 \pm 2\zeta \tag{2.49}$$

If the roots of equation (2.39) are known as ω_1 and ω_2 then;

$$4\zeta = \frac{\omega_2^2 - \omega_1^2}{\omega_n^2} \cong 2\left(\frac{\omega_2 - \omega_1}{\omega_n}\right) \tag{2.50}$$

The quantity Q is then defined as;

$$Q = \frac{\omega_n}{\omega_2 - \omega_1} = \frac{f_n}{f_2 - f_1} = \frac{1}{2\zeta} \tag{2.51}$$

Thus the damping of the system can be approximated directly from a plot of the frequency response system.

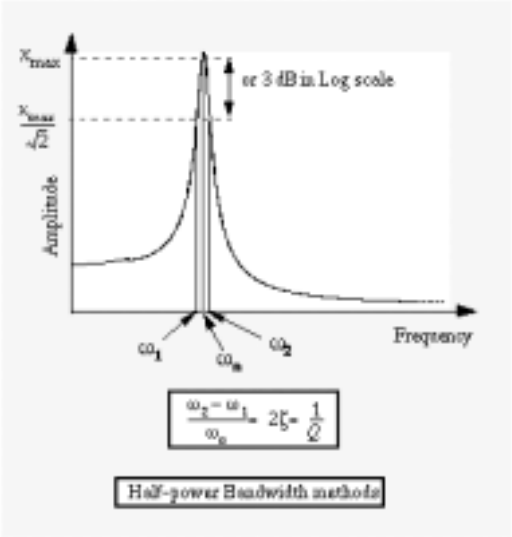

Figure 2.1 Half-Power Point Method

THIS PAGE INTENTIONALLY LEFT BLANK

III. EXPERIMENTAL SETUP

A. EQUIPMENT

- PCB Piezotronics Power Supply Model: 483B07
- PCB Piezotronics Force Sensor Model: 208C01
- PCB Piezotronics Impulse Hammer Model: 086B03
- PCB Piezotronics ICP Accelerometers Model: 336C04
- MB Dynamics Servo Amplifier Model: SS250VCF
- MB Dynamics Exciter Model: Modal 50A
- Lateral Excitation Stand Model: 2050A
- HP Digital Signal Analyzer Model: 35628
- Dell Dimension Desktop Pentium III Model: XPS T800r
- Unwelded Steel Panel (102" x 18" x 0.25")
- ½ Scale Model Watertight Bulkhead (9' x 4')
- National Instruments: LabVIEW 6.1 Virtual Instruments Software
- FORTRAN
- Microcal Origin 6.0
- MATLAB

B. EQUIPMENT SETUP

In order to test the panels in an unrestrained condition, they were suspended from a wooden support structure by eight nylon tie-down straps with hooks attached to the steel rings welded to the top of the bulkhead while the flat panel was suspended by four bungee cords. Once the panel was securely positioned, it was marked with evenly spaced numbered points where the accelerometers would be attached. A hole was drilled through the panel in order to attach the force transducer and the shaker rod.

Two methods were used to vibrate the panel. The first method was to excite the panel using the PCB modally tuned impulse hammer connected to the HP DSA. The second method used the Modal 50A exciter positioned on the lateral excitation stand such that when the exciter was connected to the panel the connecting rod was level and perpendicular to the panel. The input excitation signal was provided by the HP Digital Signal Analyzer connected to the Modal 50A exciter via the MB Dynamics Servo Amplifier. The accelerometers were numbered 1 to 5 and placed in order on the panel. The accelerometers and the force transducer attached to the shaker rod were then connected through the PCB power supply to the National Instruments Virtual Instrument

card installed in the Dell Desktop. The first accelerometer and the force transducer were also connected to the two channel HP DSA in order to measure the frequency response function of the panel and the signal coherence for a comparison with the results measured by the Virtual Instrument.

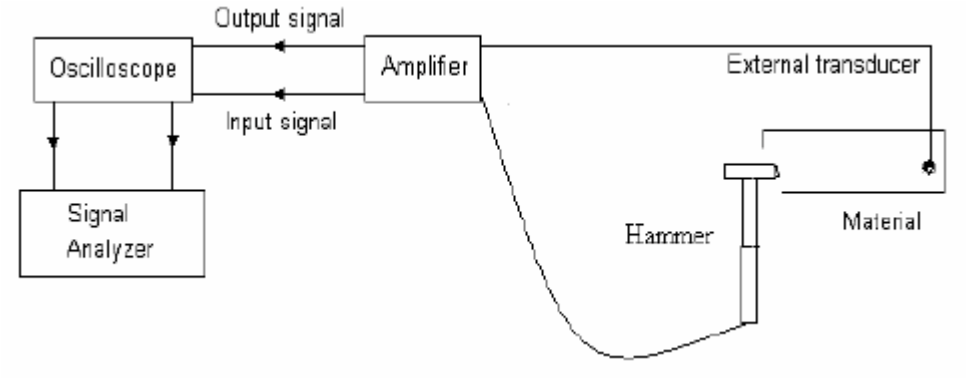

Figure 3.1 Equipment Setup for Impulse Hammer Testing

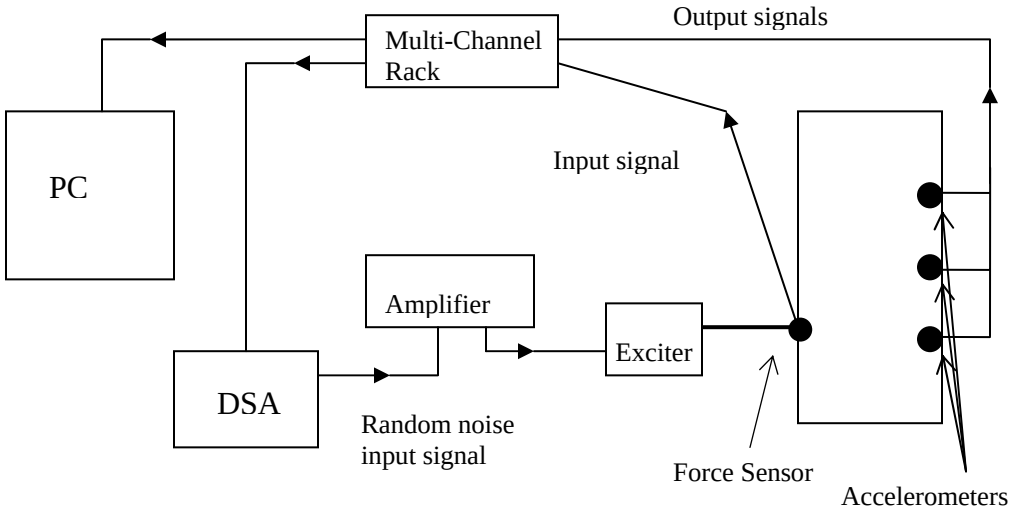

Figure 3.2 Equipment Setup for Exciter Testing

C. PANEL TESTING

1. Impulse Hammer Testing

The initial method of testing was to use the PCB modally tuned impulse hammer to excite the panel with an impact, representative of a free vibration system. Connected to the HP DSA the hammer provided the input signal while the accelerometers measured the system response. Various hammer tips were used to find one that would provide the best input signal with the least noise, resulting in a strong coherence. After the input and

output signals were amplified the HP DSA analyzed the signals to produce plots of the frequency response and coherence. The force-exponential window was used to view the plots and 10 stable mean averages were used to generate the frequency response. The trigger level for the hammer was set at 0.5 volts.

2. Exciter Testing

Instead of using the hammer to simulate a free vibration system, the exciter was used to simulate a forced vibration system. The panel as first marked with 60 numbered points where the accelerometers would be placed as in Figure 3.3. The exciter is at location 10.

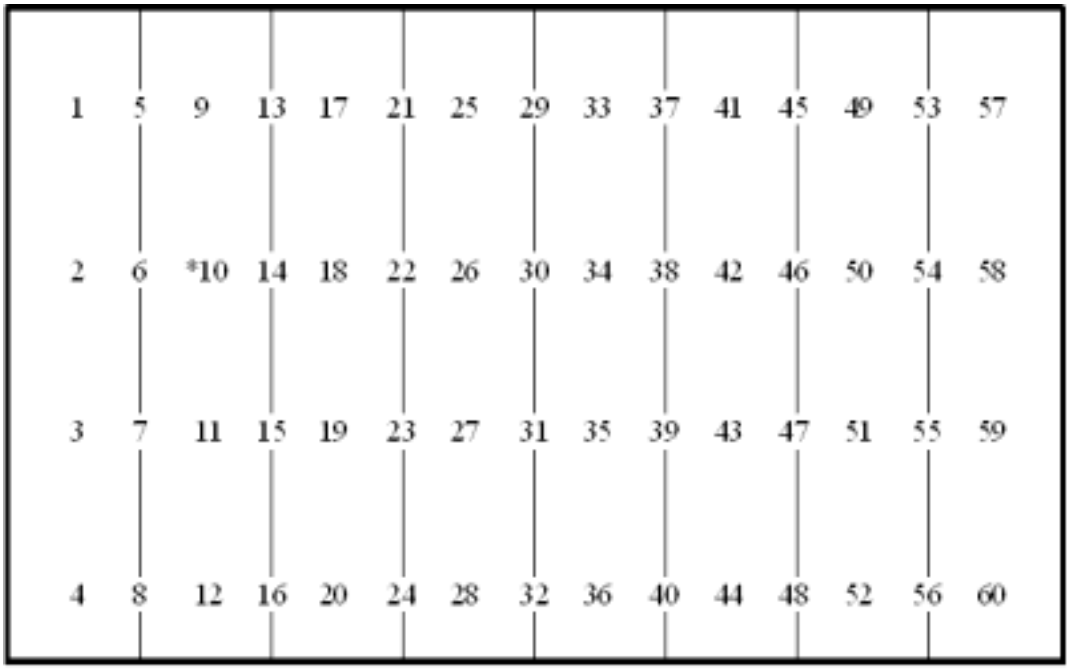

Figure 3.3 Accelerometer Positions on Watertight Bulkhead

As a first estimate of the damping, the "half-power point" method was used. The DSA generated an excitation signal or 1 volt random noise over a frequency range of 0-250 Hz. Performing a Fast Fourier Transform over 10 averages, the FRF and the coherence were plotted. Where a strong response peak was detected, the magnitude of and the frequency at which the peak occurred were recorded. Then using the X and Y scroll functions of the DSA a line was created 3 dB below the peak of the response. The intersection of this line and the response curve yielded the sideband frequencies.

Entering the peak and sideband frequencies into an EXCEL template based on the "half-power point" method yielded the first estimate of the damping between the stiffeners.

The second method of measuring the damping of the panel was to measure and record the Frequency Response Function, coherence, magnitude and phase, and the real and imaginary data. The data from the accelerometers and force transducer was recorded and processed using the Virtual Instrument 7 Channel DSA. For the initial run, the HP DSA was setup to generate random noise with a peak value of 1 volt over a frequency span of 0-250 Hz. A frequency resolution of 0.05 Hz was desired so the VI was set to record 5000 lines of data for each parameter over 10 averages. It was found that a buffer size of 20,000 and a scan rate of 100 produced the best coherence when recorded. The data was recorded as a text or .TXT file. In addition to generating the input signal, the DSA was set to record the magnitude and the FRF as measured by the first accelerometer and the force transducer. Using the data gathered from the VI, the .TXT file was then input into a FORTRAN 97 program that performed the complex exponential method and generated the damping values for a given frequency. The regenerated modal FRF and phase were then imported into Microcal Origin 6.0 and plotted with the originally measured FRF and phase as recorded by the VI. The extracted damping values and corresponding frequencies were then exported into an EXCEL spreadsheet where only the frequencies and damping values that corresponded to real modes, identified by significant peaks and phase shifts in the regenerated FRF and frequency plots, were extracted and used to create the damping versus frequency plot.

The next step was to calculate the Rayleigh damping coefficients. Using MATLAB and inputting the real and imaginary data gathered from the VI the damping coefficients α and β were calculated. Additionally the program generated a least squares curve fit of the damping values.

When the FRF over the 250 Hz range was examined, it was found that the average magnitude of the FRF between 0-20 Hz was much less than the average magnitude above 20 Hz which resulted in a poorly regenerated FRF plot in the low frequency range. To correct this, a separate test was conducted by setting the DSA to generate 1 volt random noise over a frequency span of 0-20 Hz. The VI was setup to record 400 lines of data to record at 0.05 Hz resolution. The same analysis was performed on the 0-20 Hz data as

the 0-250 Hz data. To create a more accurate picture of frequency dependent damping, the low frequency and higher frequency damping values were spliced together to cover the entire 250 Hz frequency span. For each position, data was recorded and processed for both the 0-20 Hz and the 0-250 Hz ranges

For comparison, the flat, unwelded panel was connected to the exciter and the five accelerometers were equally spaced along its length. The same testing parameters as the bulkhead were established and the data was recorded in both the 0-20 Hz and 0-250 Hz ranges.

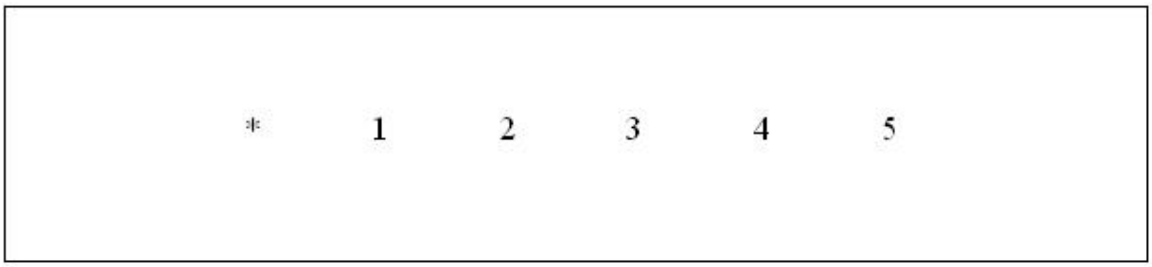

Figure 3.4 Accelerometer Positions on Unwelded Panel

D. FINITE ELEMENT MODELING

In addition to physical modeling and testing, the watertight bulkhead and the unwelded flat panel were also modeled as a finite element model in MSC Nastran/Patran. The bulkhead was modeled using 22092 quad 4 shell elements while the flat plat was modeled using 29376 quad 4 shell elements. The welds in the bulkhead were not modeled; instead the stiffeners and flat panel were merged together by "equivalencing" the mesh in Nastran/Patran. The panels were analyzed for their mode shapes at frequencies ranging from 0-250 Hz.

THIS PAGE INTENTIONALLY LEFT BLANK

IV. EXPERIMENTAL RESULTS

A. IMPACT TESTING

Although tips of varying hardness were used and many attempts were made to produce consistent impacts, the coherence values measured for the impact tests were far too low to produce accurate and reliable FRF values. As a result of these inaccurate results, impact testing was abandoned early in the experimental process in favor of the exciter testing which produced better coherence and could be easily reproduced.

B. EXCITER TESTING

1. Half-Power Point Method

The first estimate of damping values for the panel were found using the "half-power point" method as previously explained. Using the number 1 accelerometer, the force transducer, and the HP DSA to plot the magnitude response of the panel, strong resonant peaks were identified and isolated. Once isolated the frequency of the resonant peak was found as well as the frequencies of the two sidebands at 3dB below the peak magnitude. Using the equation

$$\zeta = \frac{\omega_2 - \omega_1}{2\omega_n} = \frac{f_2 - f_1}{2 f_n} \tag{4.1}$$

Table (4.1) shows the peak frequencies and the frequencies of the sidebands as well as the calculated damping values. An effort was made to use the same resonant peak as often as possible, however not every location had the same modal frequency so the analysis was performed at the resonant frequencies that had the greatest magnitude.

Table 4.1a "Half-Power Point" Results (Left Half of Bulkhead)

f1 = 114.58 **1**	f1 = 151.75 **9**	f1 = 124.5 **17**	f1 = 131.1 **25**
f2 = 144.15 ζ = **0.00376**	f2 = 151.6 ζ = **0.00099**	f2 = 124.31 ζ = **0.00149**	f2 = 130.7 ζ = **0.00305**
fn = 145.01	fn = 151.9	fn = 124.69	fn = 131.5
f1 = 160.25 **2**	f1 = 130.95 **10**	f1 = 135.8 **18**	f1 = 170.88 **26**
f2 = 160.19 ζ = **0.00045**	f2 = 130.58 ζ = **0.00277**	f2 = 135.71 ζ = **0.00050**	f2 = 170.6 ζ = **0.00168**
fn = 160.33	fn = 131.3 **Shaker**	fn = 135.85	fn = 171.18
f1 = 156.23 **3**	f1 = 160.18 **11**	f1 = 160.23 **19**	f1 = 130.98 **27**
f2 = 155.6 ζ = **0.00376**	f2 = 160.09 ζ = **0.00050**	f2 = 160.16 ζ = **0.00037**	f2 = 130.63 ζ = **0.00277**
fn = 156.78	fn = 160.25	fn = 160.28	fn = 131.35
f1 = 156.23 **4**	f1 = 169.15 **12**	f1 = 131.08 **20**	f1 = 169.05 **28**
f2 = 155.7 ζ = **0.00312**	f2 = 168.96 ζ = **0.00107**	f2 = 130.73 ζ = **0.00269**	f2 = 168.8 ζ = **0.00148**
fn = 156.68	fn = 169.33	fn = 131.43	fn = 169.3

Table 4.1b "Half-Power Point" Results (Right Half of Bulkhead)

f1 = 135.55 **33**	f1 = 140.2 **41**	f1 = 140.2 **49**	f1 = 148.93 **57**
f2 = 135.45 ζ = **0.00066**	f2 = 139.98 ζ = **0.00168**	f2 = 139.9 ζ = **0.00209**	f2 = 148.76 ζ = **0.00105**
fn = 135.63	fn = 140.45	fn = 140.49	fn = 149.08
f1 = 159.93 **34**	f1 = 151.71 **42**	f1 = 140.3 **50**	f1 = 160.25 **58**
f2 = 159.83 ζ = **0.00059**	f2 = 151.54 ζ = **0.00105**	f2 = 140.01 ζ = **0.00214**	f2 = 160.16 ζ = **0.00051**
fn = 160.01	fn = 151.86 **Shaker**	fn = 140.61	fn = 160.33
f1 = 159.85 **35**	f1 = 151.58 **43**	f1 = 170.83 **51**	f1 = 140.25 **59**
f2 = 159.76 ζ = **0.00063**	f2 = 151.45 ζ = **0.00082**	f2 = 170.55 ζ = **0.00154**	f2 = 139.98 ζ = **0.00196**
fn = 159.96	fn = 151.7	fn = 171.08	fn = 140.53
f1 = 150.83 **36**	f1 = 169.28 **44**	f1 = 140 **52**	f1 = 140.25 **60**
f2 = 150.65 ζ = **0.00120**	f2 = 169.02 ζ = **0.00157**	f2 = 139.7 ζ = **0.00214**	f2 = 139.98 ζ = **0.00196**
fn = 151.01	fn = 169.55	fn = 140.3	fn = 140.53

The above table shows the results of the "half-power point" testing. Although the damping values vary across the panel, the damping is never greater than 0.4%.

2. Modal Parameter Extraction

After completing an initial estimation of the damping using the "half-power point" method a more accurate and robust method for calculating the damping was used. The National Instruments LabVIEW software was used to perform Fast Fourier Transforms on the input data from the force transducer and the output data from the accelerometers. The resulting magnitude, phase, real, imaginary, and coherence data was exported to FORTRAN via a .TXT file. The FORTRAN code calculated the modal parameters for each position using the complex exponential method explained in Chapter II. The extracted modal parameters were then imported into Microcal Origin 6.0 where the damping values, original and regenerated FRF and phase curves were plotted. Comparing the original and regenerated FRF curves, the frequencies and corresponding damping values of the most resonant modes (large, narrow banded peaks) were exported to an EXCEL spreadsheet.

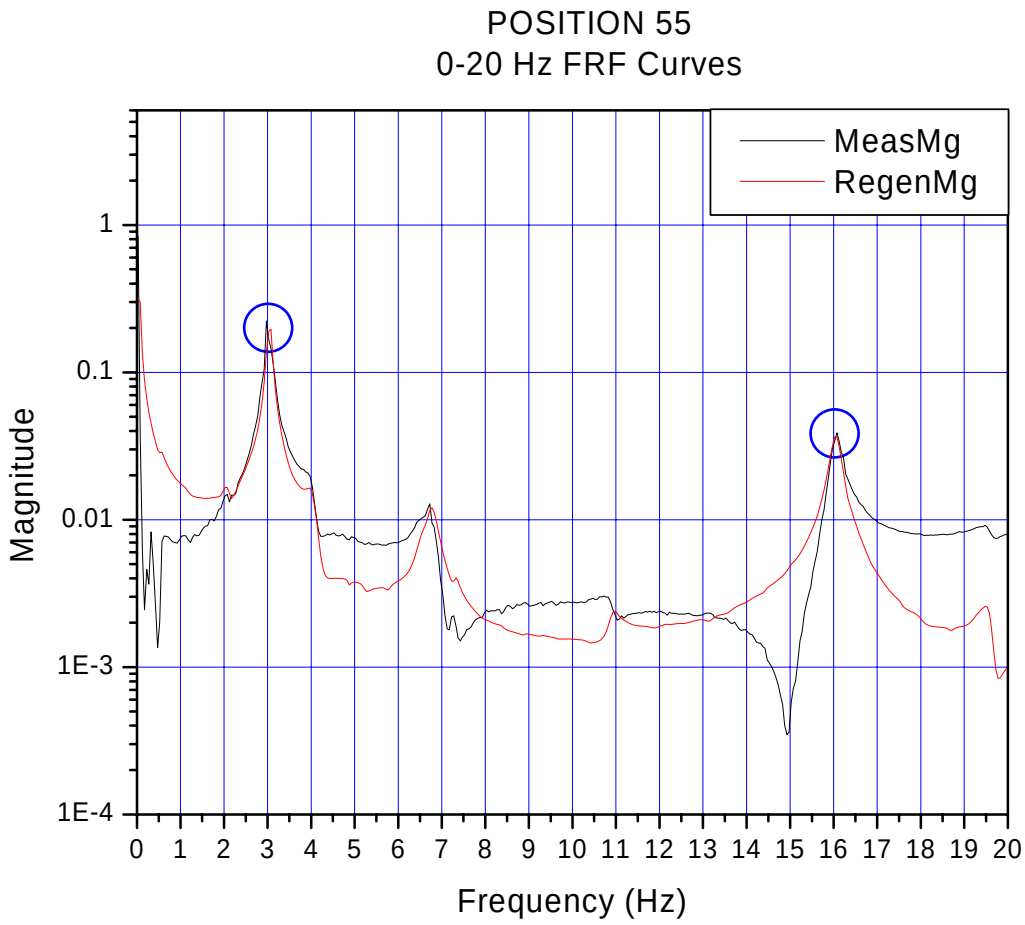

*Blue circles indicate true modal responses

Figure 4.1 Position 55 0-20 Hz FRF Curves

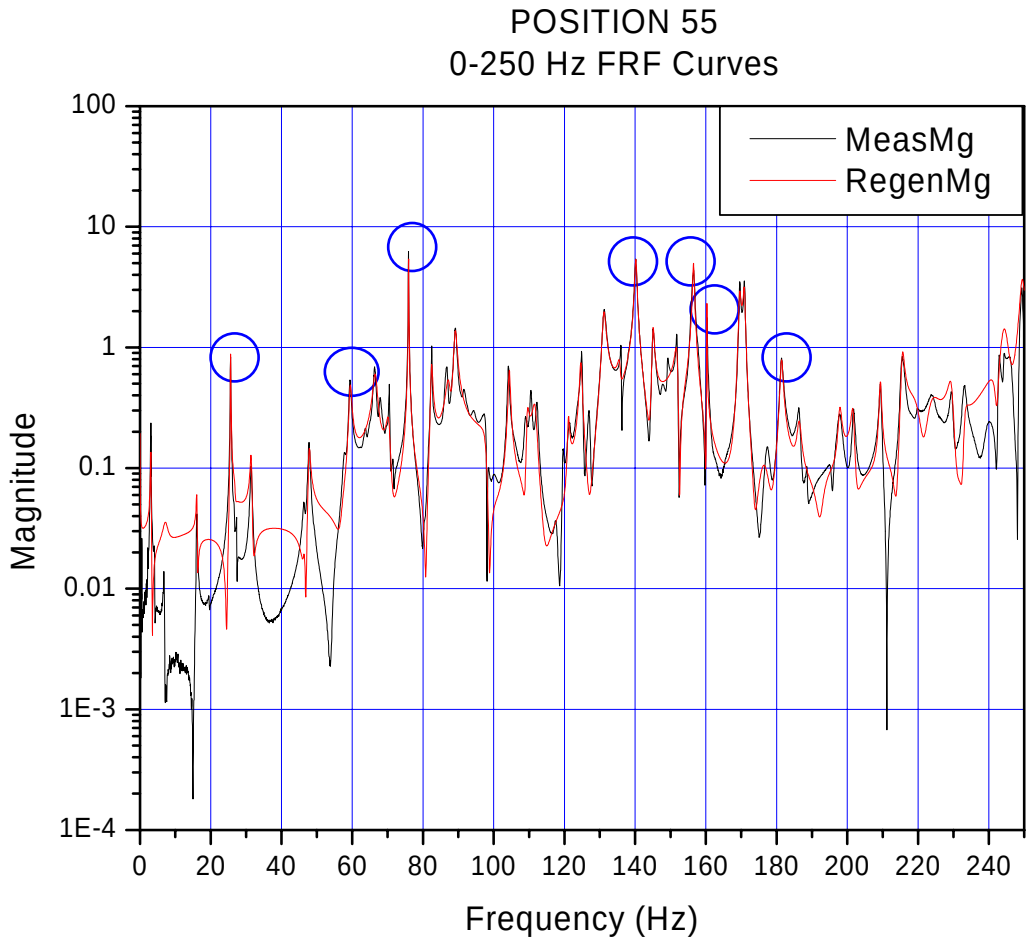

*Blue circles indicate true modal responses

Figure 4.2 Position 55 0-250 Hz FRF Curves

Once imported into the EXCEL spreadsheet the damping values over a range of frequencies as well as at a particular frequency over a range of locations could be plotted. Finally, the Rayleigh damping coefficients α and β and a least squares curve fit of the damping at each location was performed using MATLAB and the theory mentioned in Chapter II.

a. Damping for Horizontal Positions

The objective of this investigation was to determine the effects welds have on structural damping. If welds do result in higher damping, then measuring the damping at a point as far from the exciter as possible, in other words the damping should increase

as the number of welds between the location of the source and measurement location increases. To test this theory, damping measurements were calculated for the locations horizontal to the exciter, as shown in the blue box in Figure 4.3.

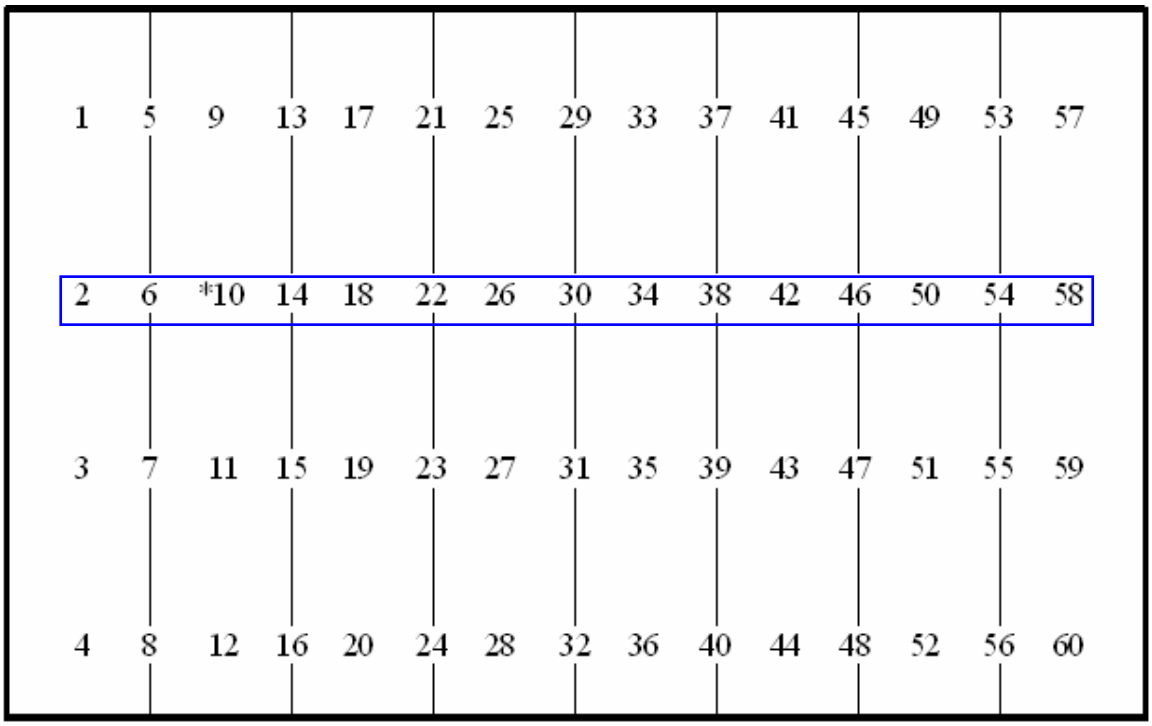

Figure 4.3 Measurement Locations for Horizontal Damping

Figure 4.4 shows the damping value of each position over the frequency range of 0-250 Hz.

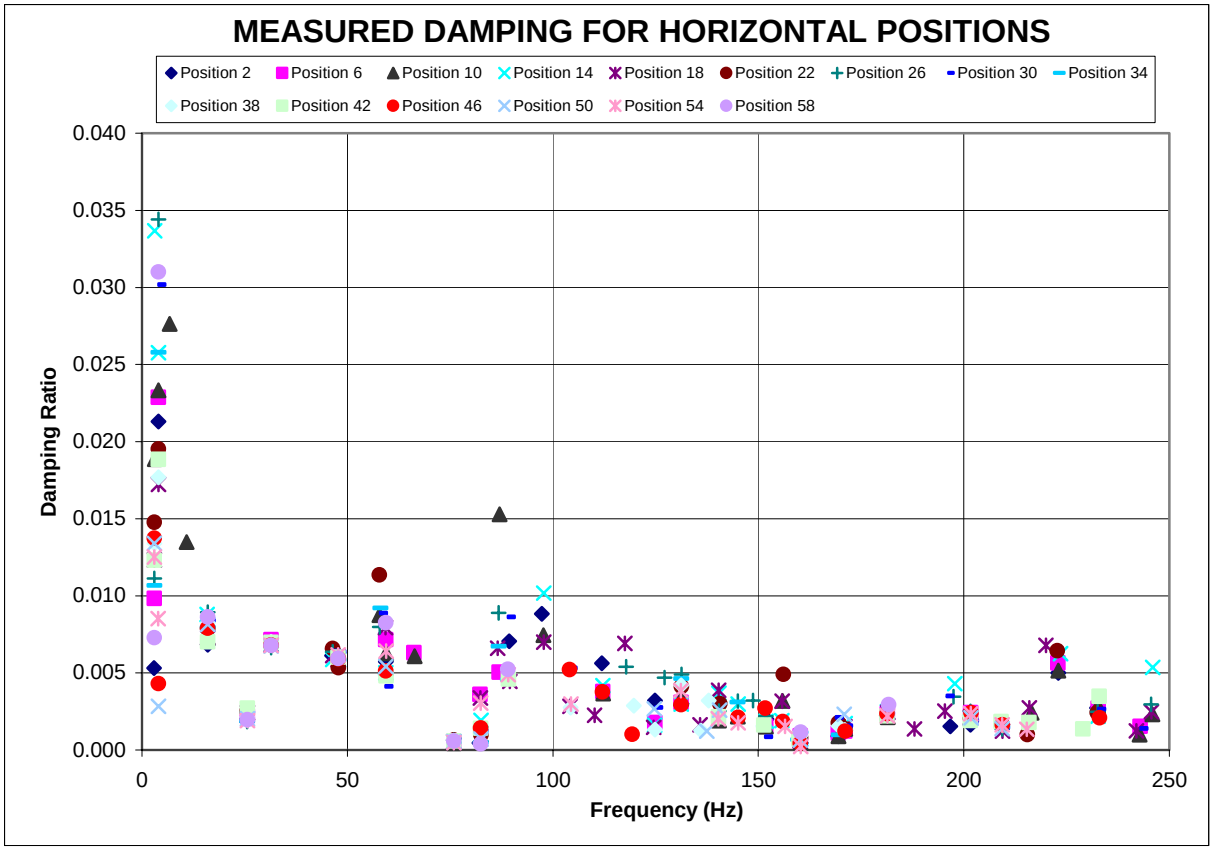

Figure 4.4 Measured Damping Values for Horizontal Positions

It is clear that the damping is dependent on the frequency as the damping values decrease exponentially as the frequency of the input increases. However it is difficult to determine how much the welds contribute to the damping. To determine the effects of the welds, the damping values for these positions were calculated at five modal frequencies; 16, 59, 76, 181, and 201 Hz. Plotting the damping at each modal frequency versus location (inches from the left edge), gave the following results.

Table 4.2 Damping at Modal Frequencies for Horizontal Positions

POSITION	DISTANCE	DAMPING FOR GIVEN MODAL FREQUENCY				
		16 Hz	59 Hz	76 Hz	181 Hz	201 Hz
2	6.63	0.00683	0.00572	0.00064		0.00163
6	13.25		0.00715	0.00045	0.00235	0.00241
10	19.88	0.00728	0.00626	0.00044	0.00214	
14	26.50	0.00878	0.00501	0.00054	0.00249	
18	33.13	0.00727	0.00795	0.00054	0.00244	0.00214
22	39.75	0.00789		0.00065		0.00206
26	46.38	0.00894	0.00499	0.00063	0.00223	0.00250
30	53.00	0.00839	0.00411	0.00068	0.00238	0.00190
34	59.63	0.00797	0.00492	0.00052		
38	66.25	0.00825		0.00061		0.00224
42	72.88	0.00702	0.00479	0.00057	0.00222	0.00190
46	79.50	0.00791	0.00512		0.00235	0.00243
50	86.13	0.00815	0.00542	0.00054		0.00208
54	92.75		0.00642	0.00048	0.00221	0.00235

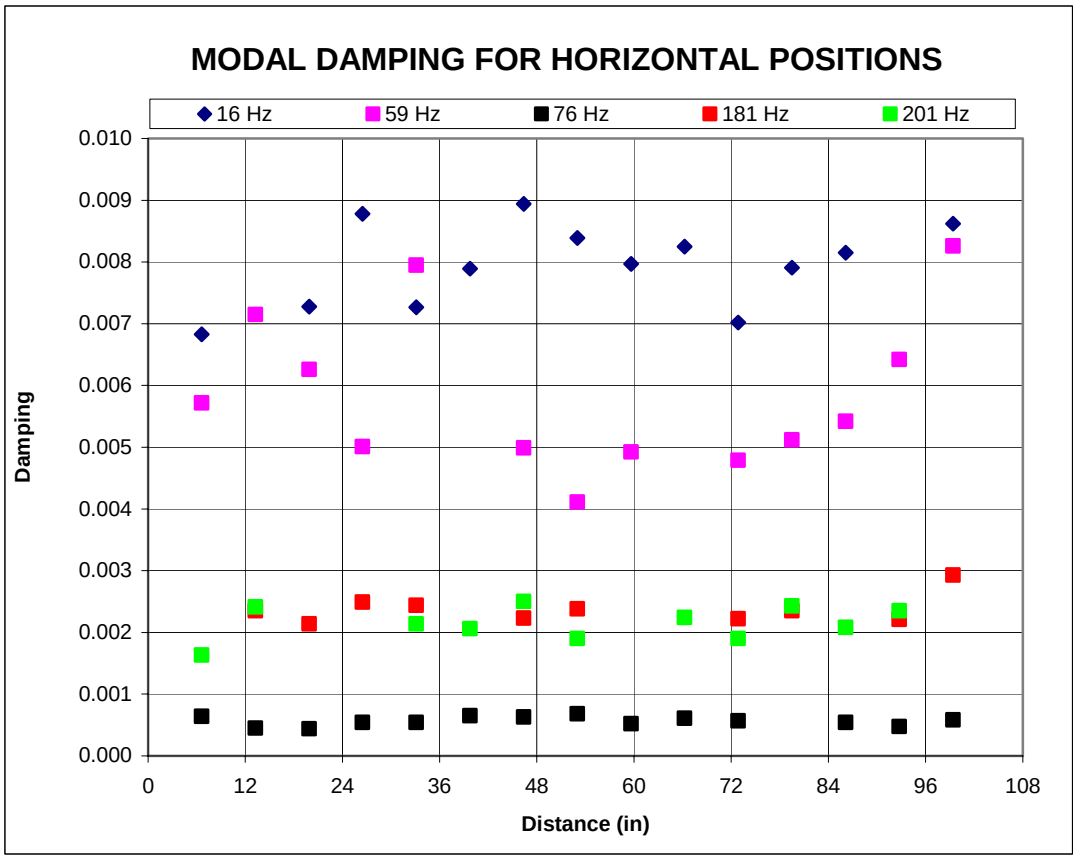

Figure 4.5 Modal Damping for Horizontal Positions

From Figure 4.5 it is clear that the damping is not as strongly affected by the distance from the source or the number of welds between the measurement and the source, but rather the damping is more dependent on the frequency of the excitation. The lower frequency excitation (16 Hz and 59 Hz) produced higher damping values with more variation than the damping at higher frequencies (76 Hz, 181 Hz, and 201 Hz) which had a much lower level of damping with less variation.

The calculated Rayleigh damping coefficients are listed in Table 4.3 and the best fit curve of Rayleigh damping compared to the originally measured damping values is shown for each position in the following plots.

Table 4.3 Rayleigh Damping Coefficients for Horizontal Positions

Position	α	β	Position	α	β
2	0.55383	5.64E-06	34	0.76510	4.90E-06
6	0.67804	4.48E-06	38	0.68501	3.80E-06
10	1.13142	4.60E-06	42	0.68214	3.43E-06
14	1.34924	5.27E-06	46	0.46035	4.26E-06
18	0.66848	5.06E-06	50	0.42024	3.67E-06
22	0.76415	5.04E-06	54	0.48189	4.24E-06
26	0.93907	4.91E-06	58	0.77911	6.74E-06
30	1.56177	3.42E-06			

The average α value for the horizontal positions was 0.795 with a standard deviation of 0.327 and the average β value was 4.631E-6 with a standard deviation of 8.950E-7.

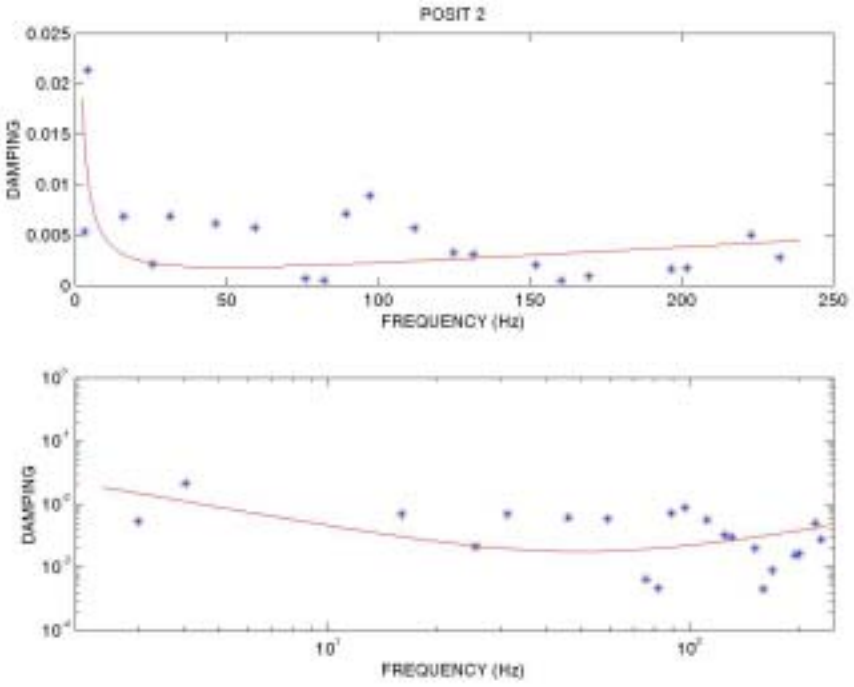

Figure 4.6 Best Fit & Rayleigh Damping Curves for Bulkhead Position 2

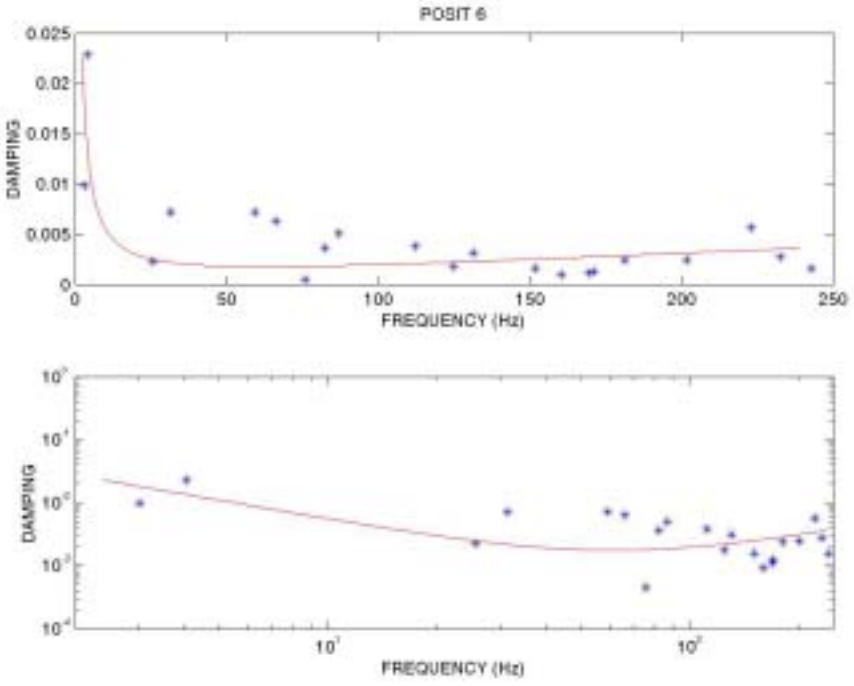

Figure 4.7 Best Fit & Rayleigh Damping Curves for Bulkhead Position 6

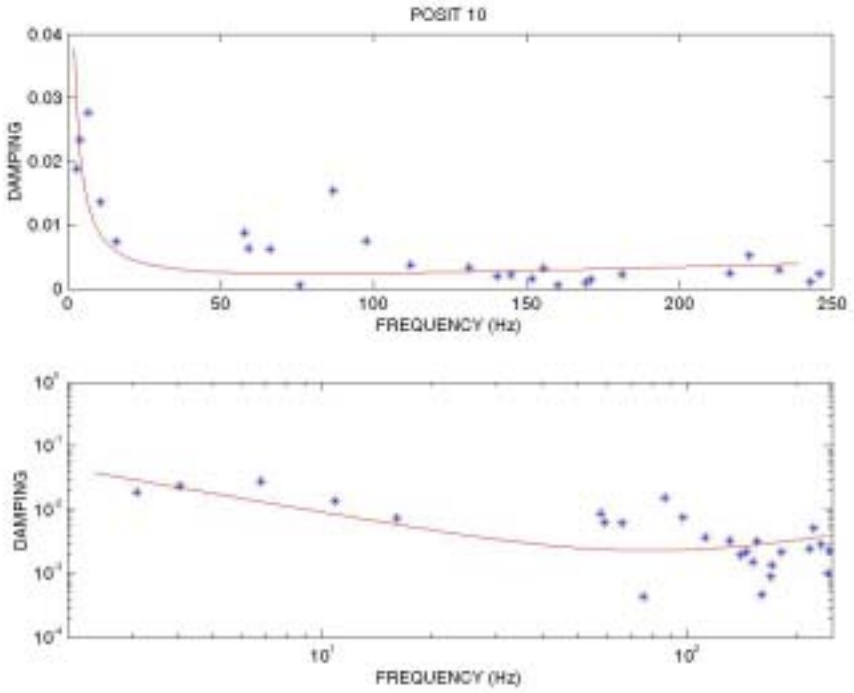

Figure 4.8 Best Fit & Rayleigh Damping Curves for Bulkhead Position 10

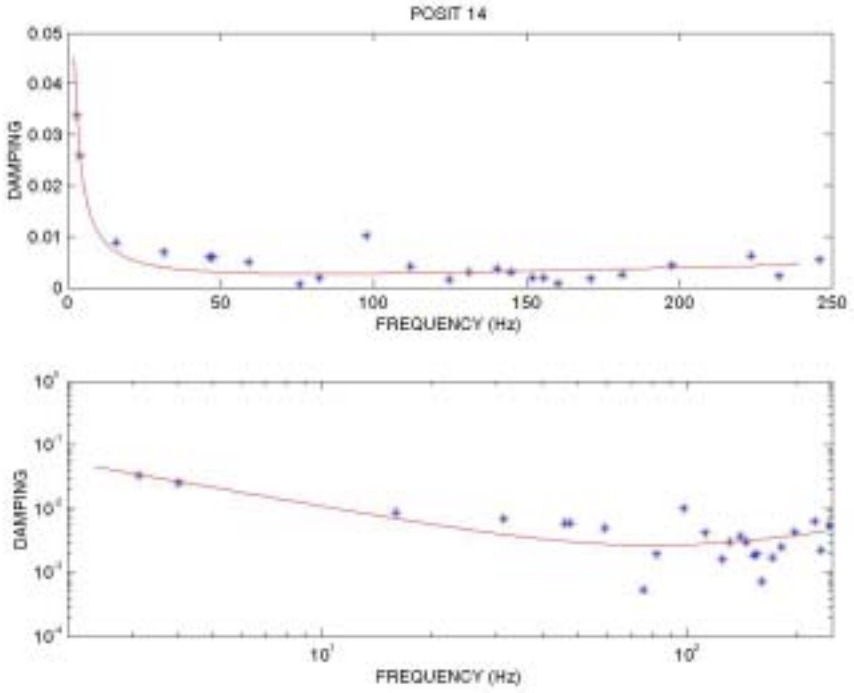

Figure 4.9 Best Fit & Rayleigh Damping Curves for Bulkhead Position 14

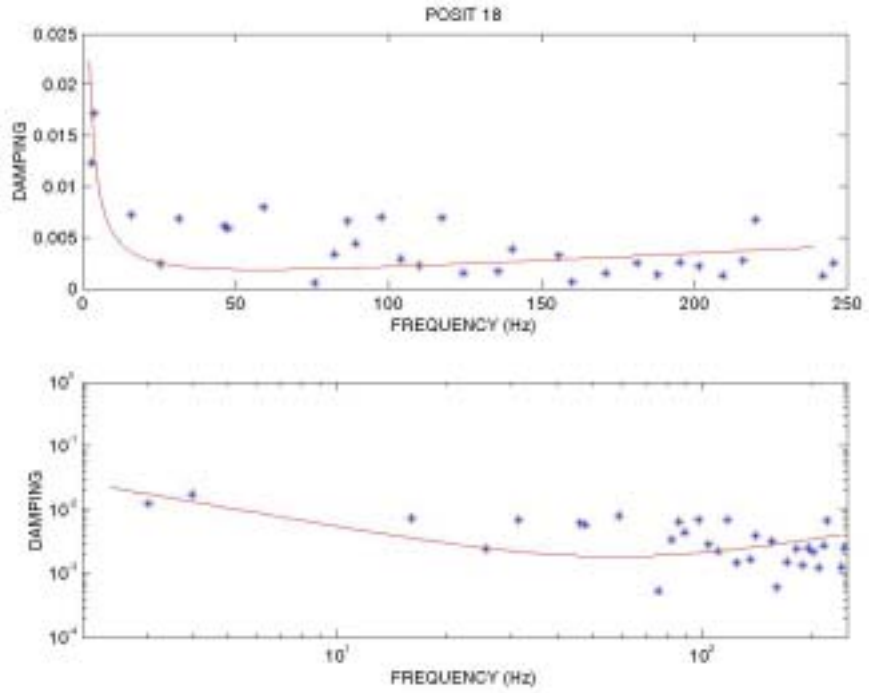

Figure 4.10 Best Fit & Rayleigh Damping Curves for Bulkhead Position 18

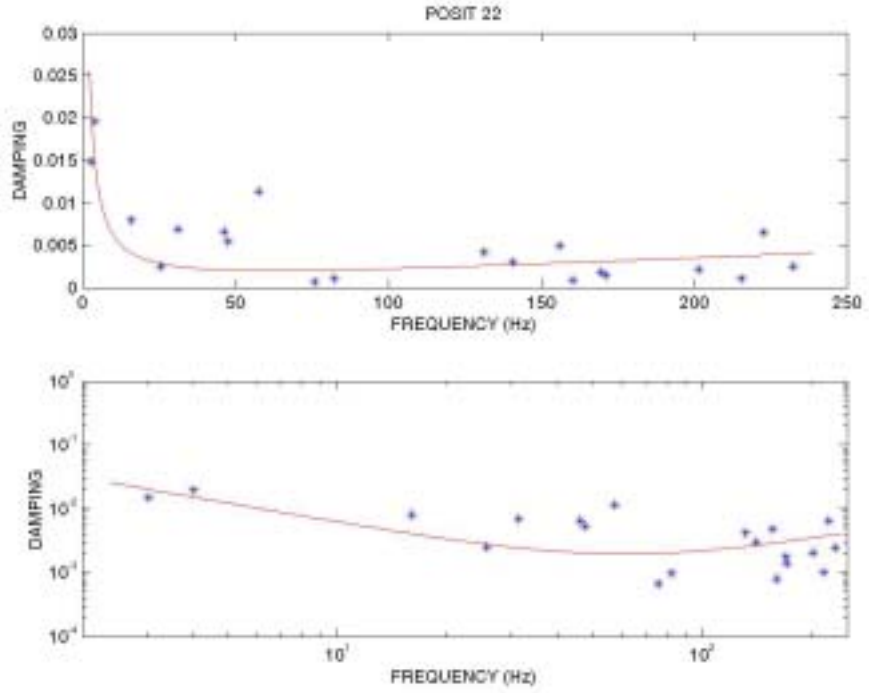

Figure 4.11 Best Fit & Rayleigh Damping Curves for Bulkhead Position 22

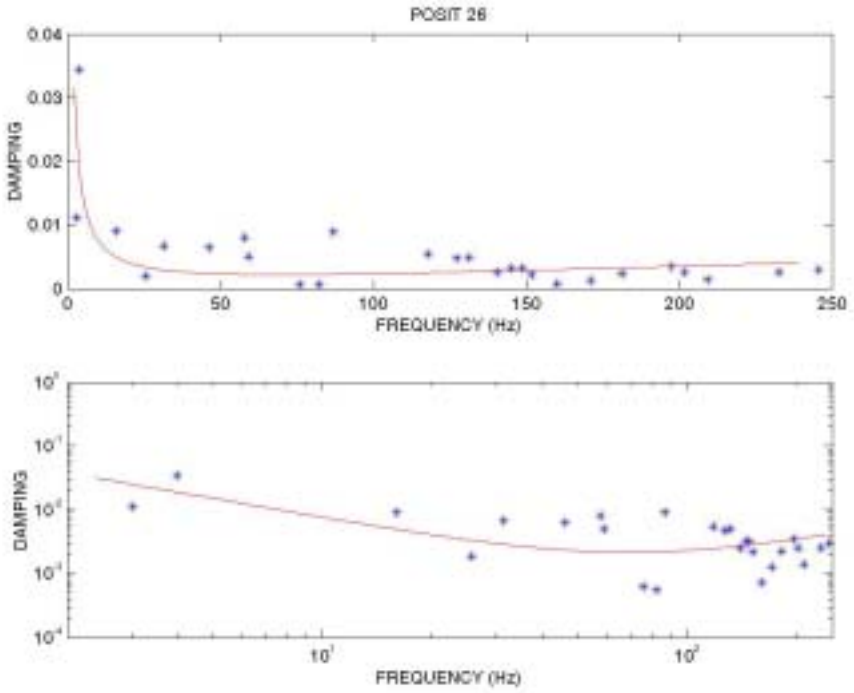

Figure 4.12 Best Fit & Rayleigh Damping Curves for Bulkhead Position 26

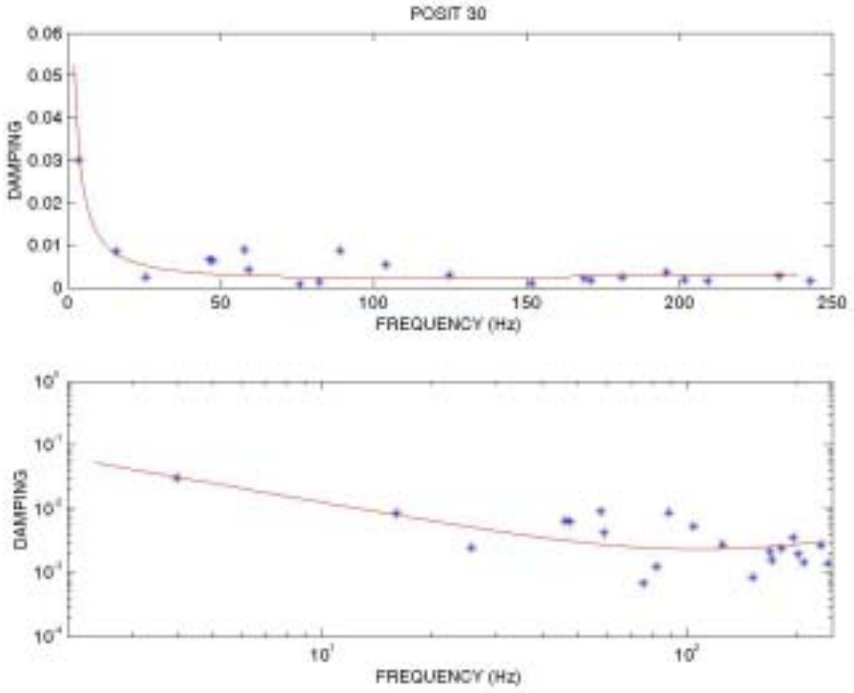

Figure 4.13 Best Fit & Rayleigh Damping Curves for Bulkhead Position 30

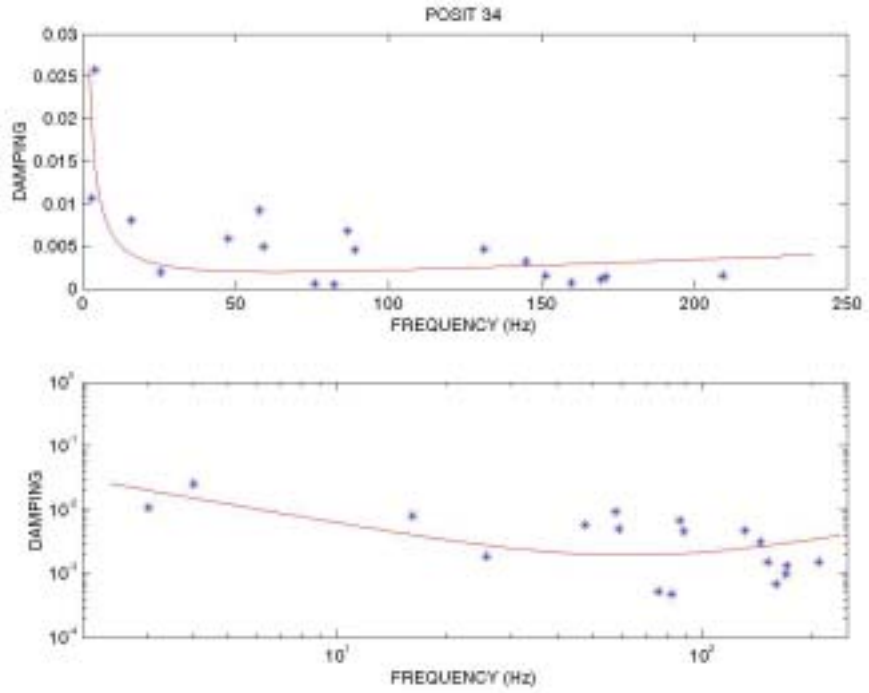

Figure 4.14 Best Fit & Rayleigh Damping Curves for Bulkhead Position 34

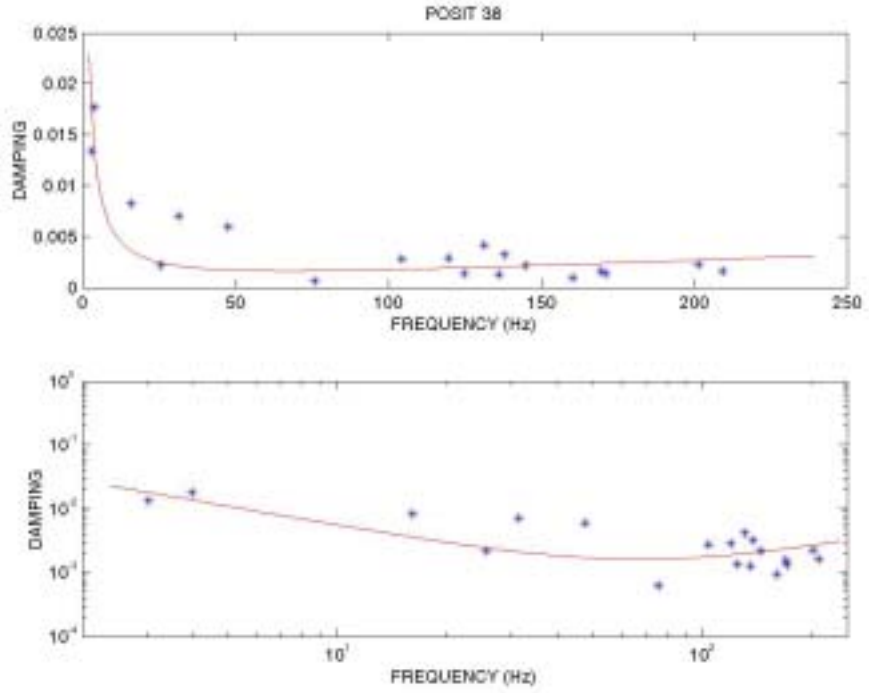

Figure 4.15 Best Fit & Rayleigh Damping Curves for Bulkhead Position 38

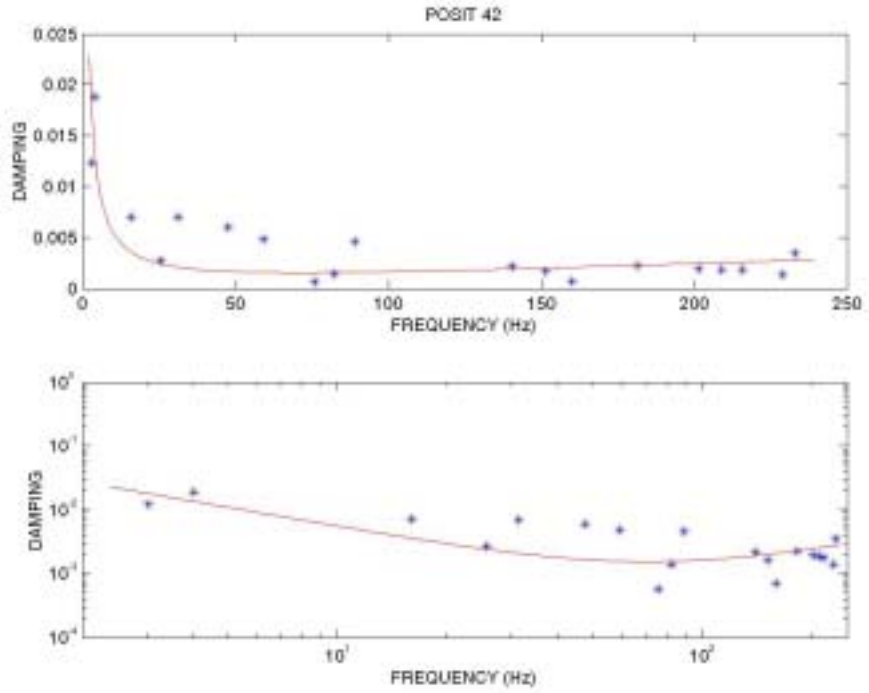

Figure 4.16 Best Fit & Rayleigh Damping Curves for Bulkhead Position 42

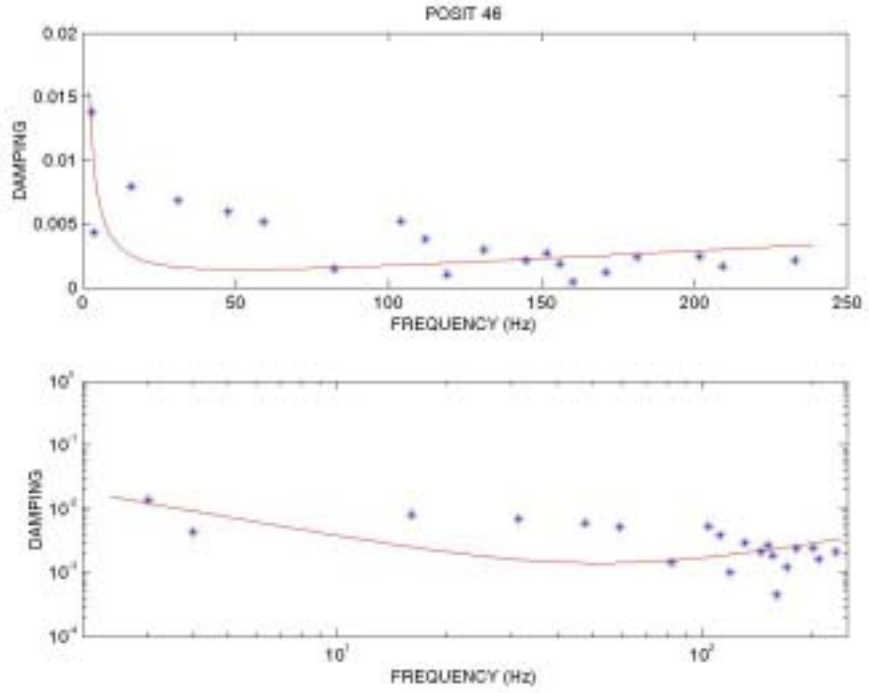

Figure 4.17 Best Fit & Rayleigh Damping Curves for Bulkhead Position 46

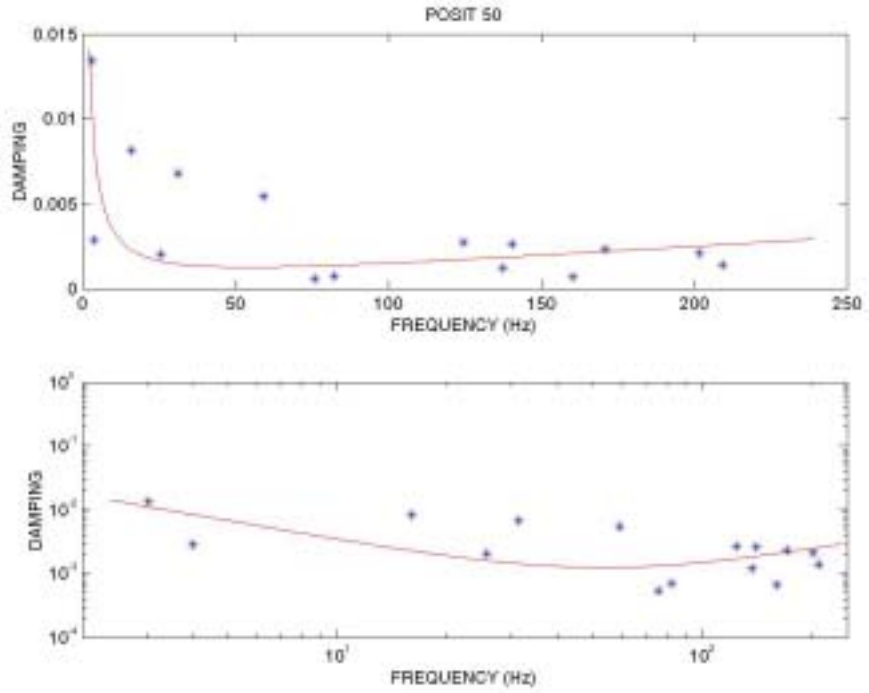

Figure 4.18 Best Fit & Rayleigh Damping Curves for Bulkhead Position 50

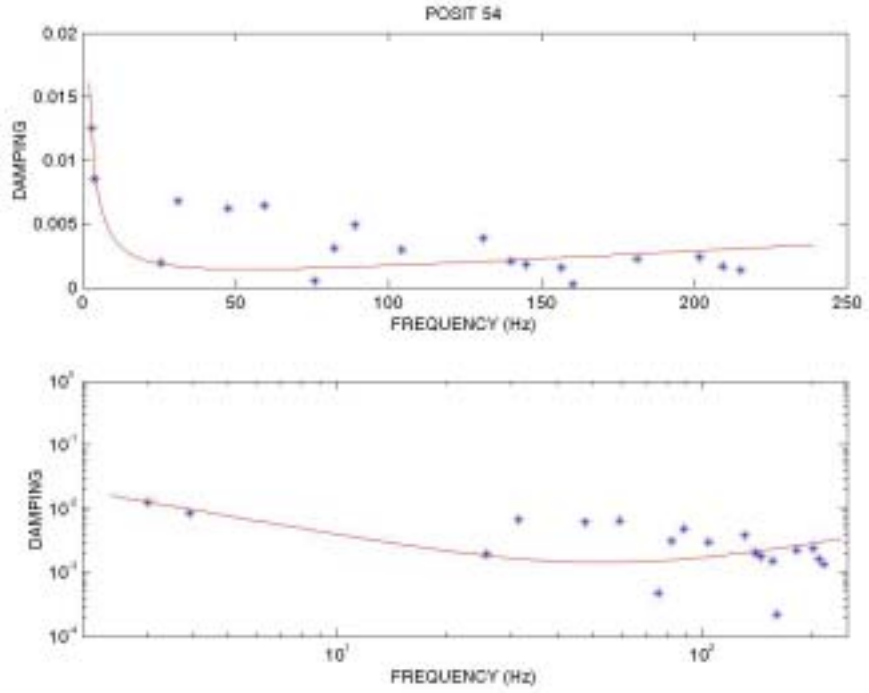

Figure 4.19 Best Fit & Rayleigh Damping Curves for Bulkhead Position 54

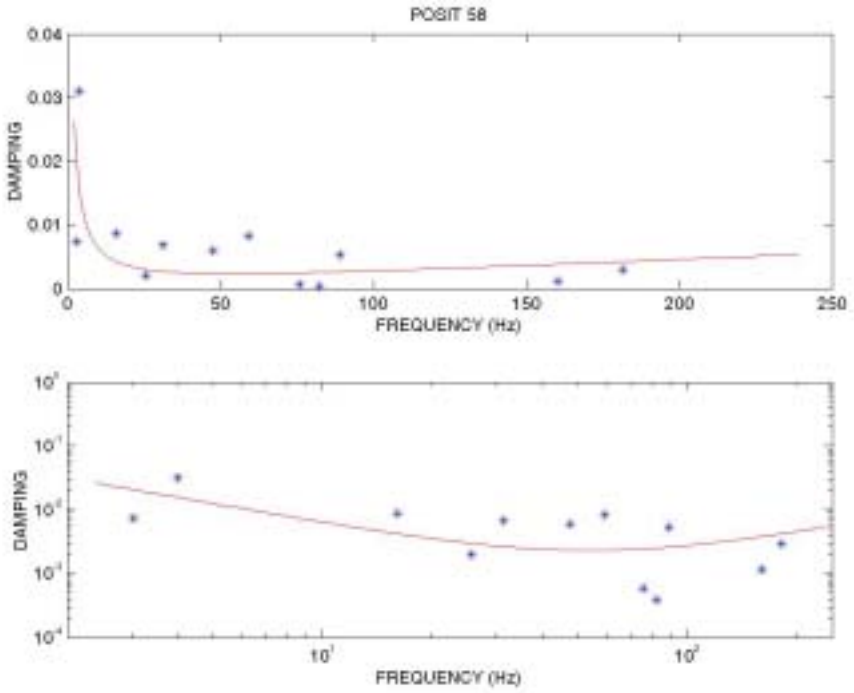

Figure 4.20 Best Fit & Rayleigh Damping Curves for Bulkhead Position 58

b. Damping for Vertical Positions

Damping values of the panel were also taken in the vertical direction in the same section as the exciter as shown in Figure 4.21

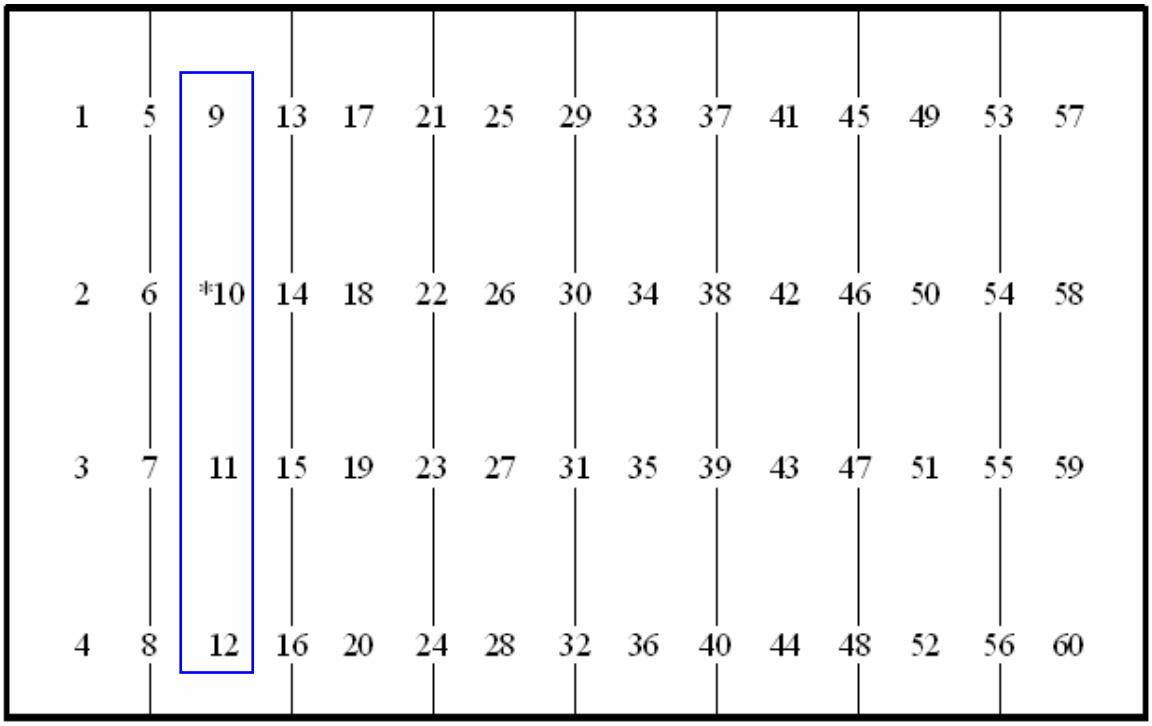

Figure 4.21 Measurement Locations for Vertical Damping

Figure 4.22 gives the measured damping values for each position over the 0-250 Hz range.

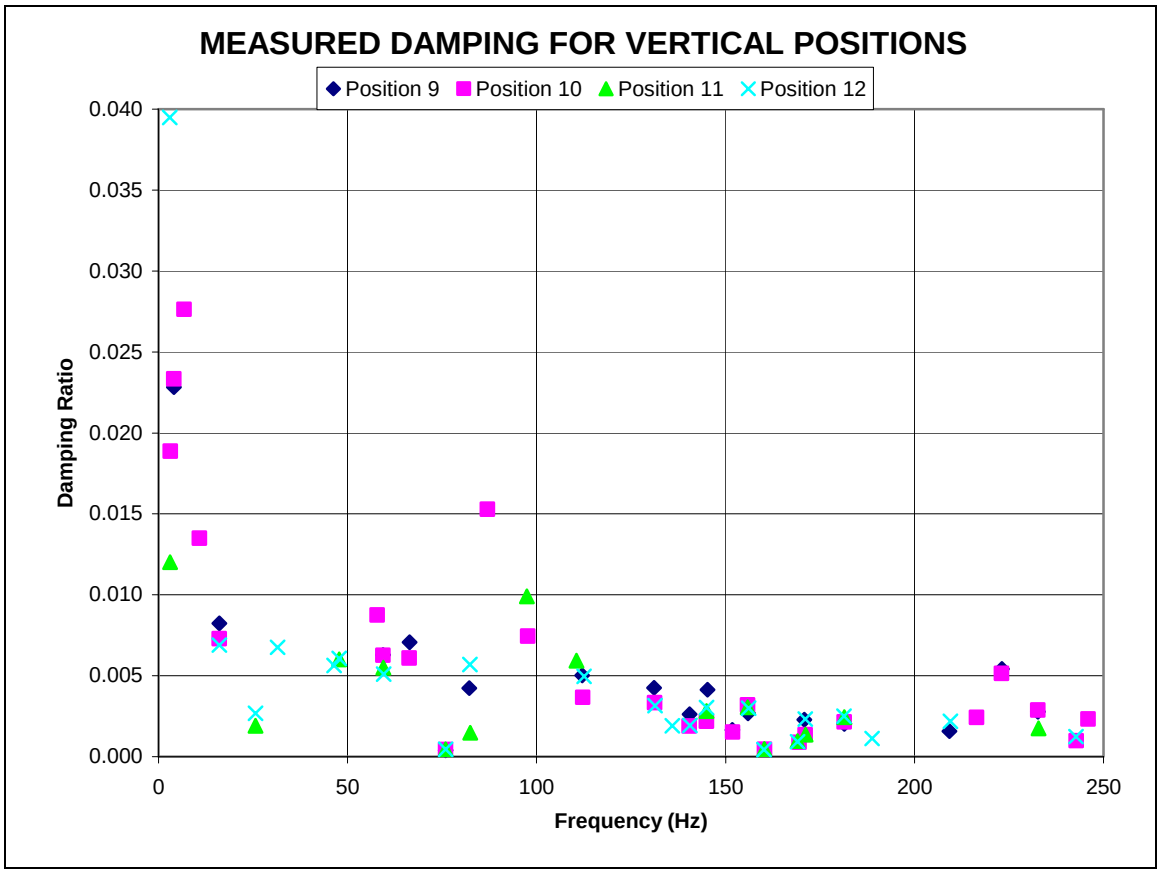

Figure 4.22 Measured Damping Values for Vertical Positions

Similar to the trend in damping values for the positions across the panel, the vertical damping values in Figure 4.22 show the same exponential decay as the frequency increases. Although there are no welds between any of the measurement points and the exciter it is still important to check if the location at which the measurements were taken has any affect on the damping values. Plotting the damping values as a function of location for the modal frequencies (16, 59, 76, 181, and 232 Hz), shows that it is more likely that the damping is more likely a function of the frequency than the location on the bulkhead.

Table 4.4 Damping at Modal Frequencies for Vertical Positions

Position	Distance	Damping at Modal Frequency				
		16 Hz	59 Hz	76 Hz	181 Hz	232 Hz
9	6	0.00823	0.00629	0.00040	0.00203	0.00278
10	18	0.00728	0.00626	0.00044	0.00214	0.00287
11	30		0.00550	0.00046	0.00244	0.00175
12	42	0.00689	0.00510	0.00046	0.00251	

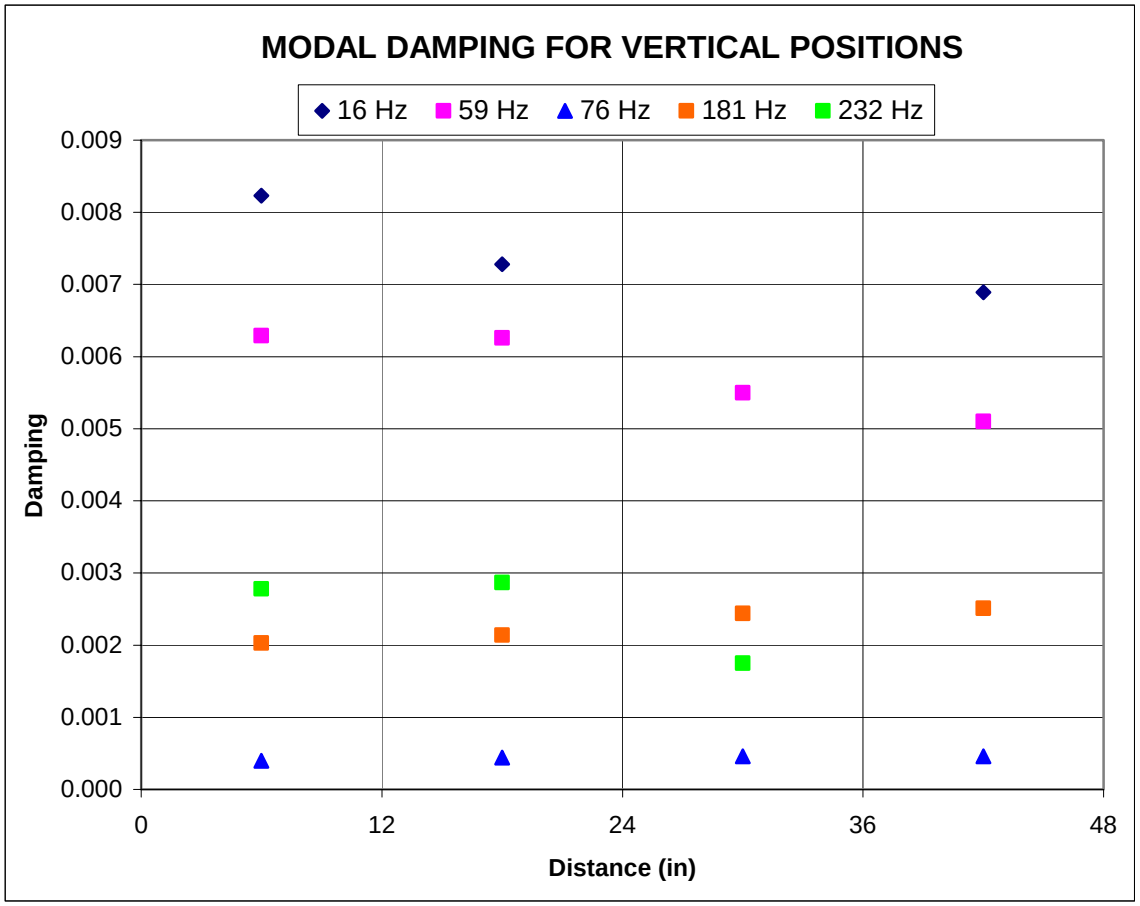

Figure 4.23 Modal Damping Values for Vertical Positions

Figure 4.23 shows for each position the damping value varies from 0.5-0.8% for the low frequencies with some variation as the location changes. For the higher frequencies the damping value decreases significantly but the damping values for the different locations changes fairly little.

The calculated Rayleigh damping coefficients are listed in Table 4.5 and the best fit curve of Rayleigh damping compared to the originally measured damping values is shown for each position in the following plots.

Table 4.5 Rayleigh Damping Coefficients for Vertical Positions

Position	α	β
9	1.21250	5.03E-06
10	1.13142	4.60E-06
11	0.48038	5.09E-06
12	1.46744	3.08E-06

The α coefficients have a mean value of 1.073 with a standard deviation of 0.420 while the β coefficients have mean value of 4.450E-6 with a standard deviation of 9.398E-7.

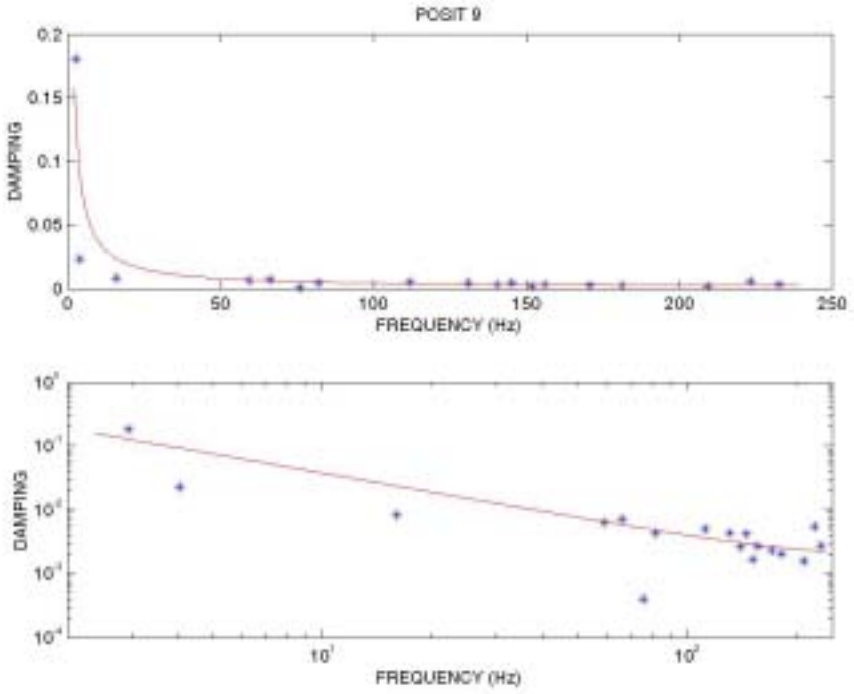

Figure 4.24 Best Fit & Rayleigh Damping Curves for Bulkhead Position 9

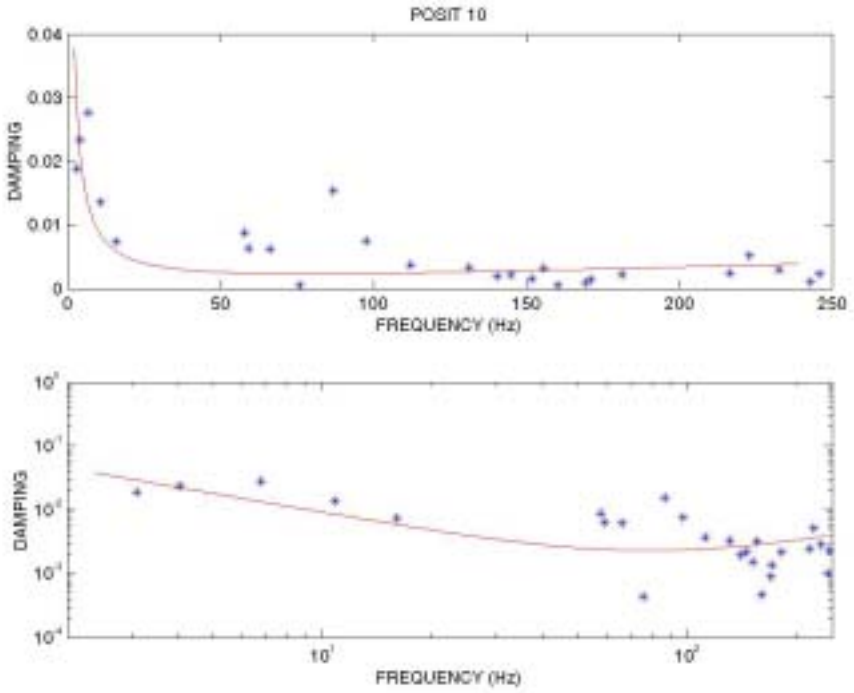

Figure 4.25 Best Fit & Rayleigh Damping Curves for Bulkhead Position 10

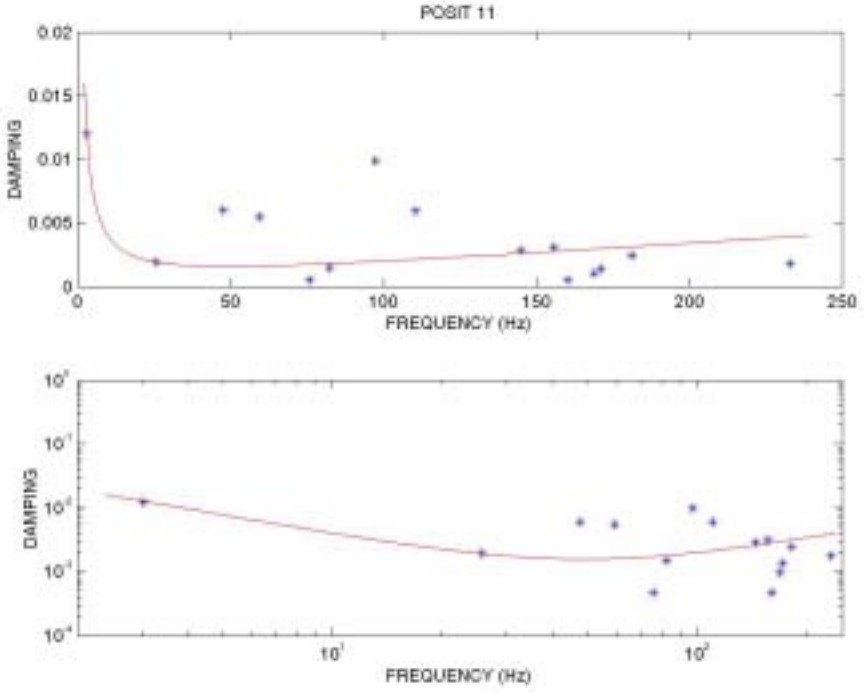

Figure 4.26 Best Fit & Rayleigh Damping Curves for Bulkhead Position 11

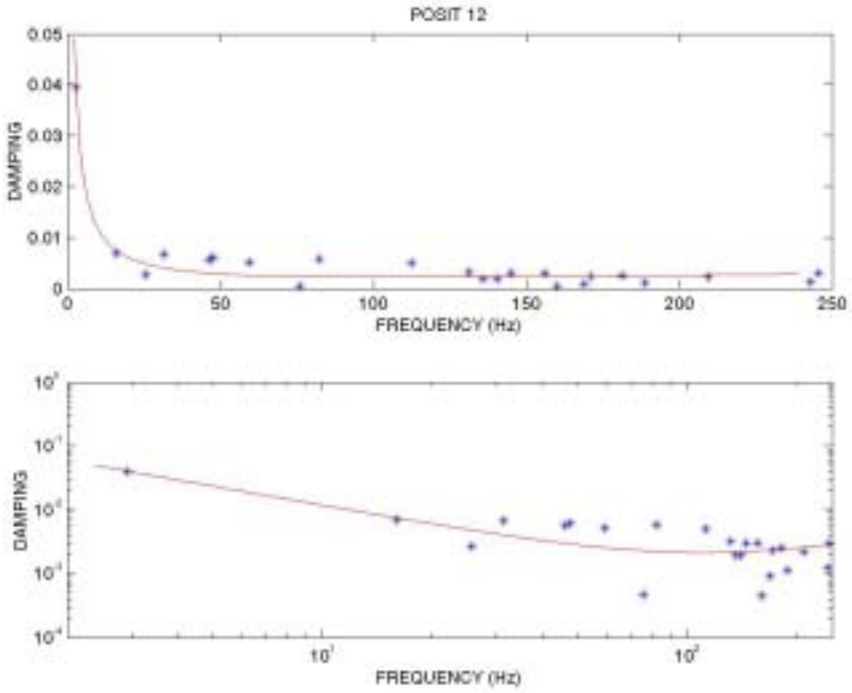

Figure 4.27 Best Fit & Rayleigh Damping Curves for Bulkhead Position 12

c. Damping for Panel Center

Damping values were also calculated for a region in the center of the panel, as indicated in Figure 4.28.

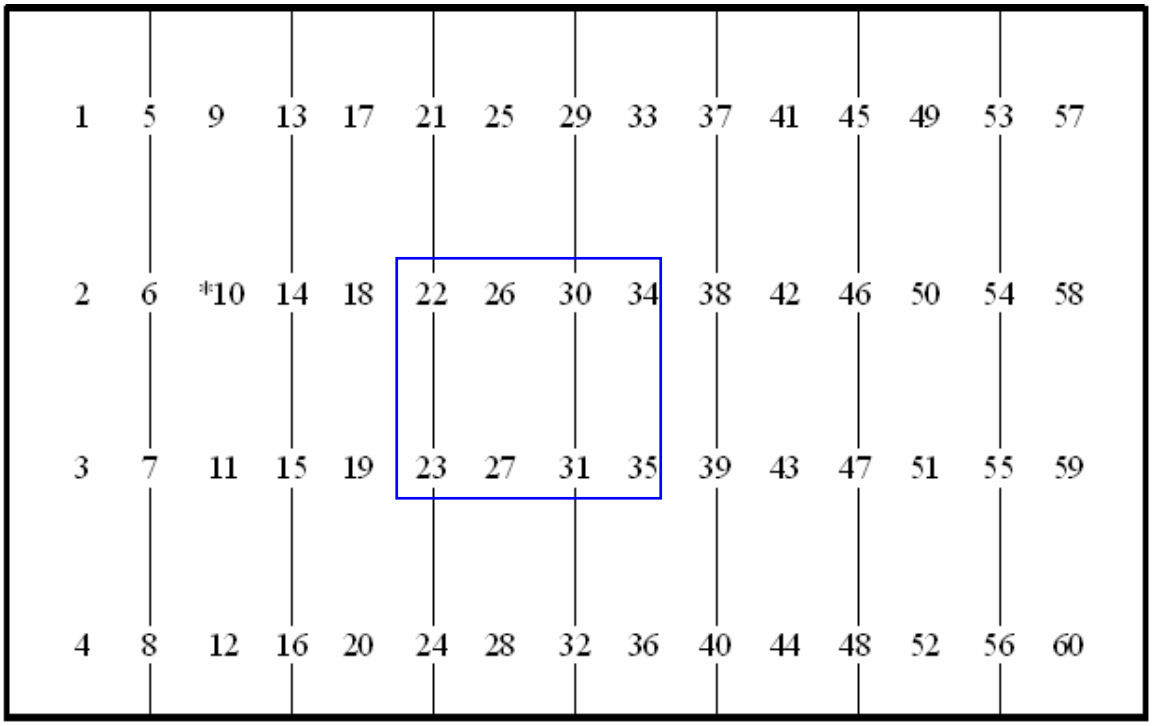

Figure 4.28 Measurement Locations for Damping in Panel Center

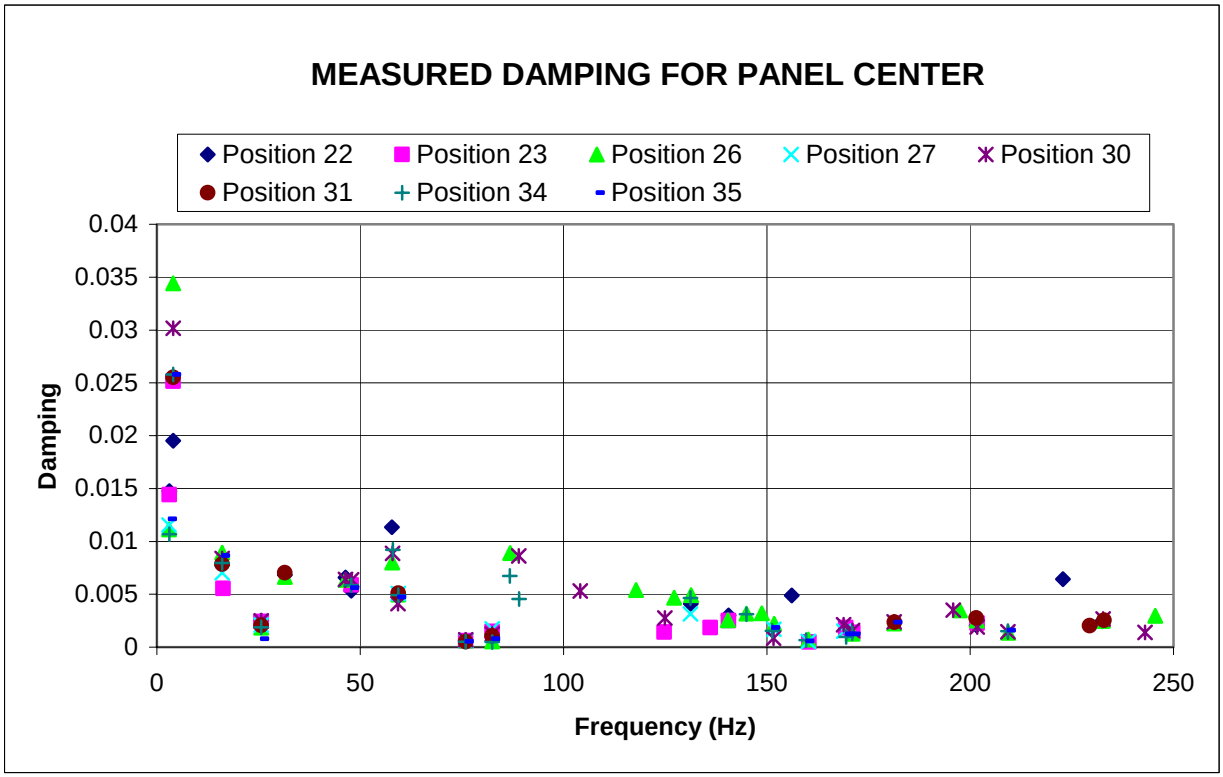

Figure 4.29 Measured Damping Values for Panel Center

Once again the damping is seen to be strongly related to the frequency of the excitation. The damping values appear greatest at low frequencies regardless of position and appear the least at higher frequencies. Checking the damping values of these positions at specific frequencies (16, 25, 76, 82, and 232 Hz) will show the relationship between damping, frequency, welds and location.

Table 4.6 Damping at Modal Frequencies for Panel Center

Position	Damping at Modal Frequencies				
	16 Hz	25 Hz	76 Hz	82 Hz	232 Hz
22	0.00789	0.00251	0.00065	0.00098	0.00243
23	0.00555	0.00241	0.00060	0.00149	
26	0.00894	0.00185	0.00063	0.00055	0.00248
27	0.00703	0.00209	0.00064	0.00173	
30	0.00839	0.00247	0.00068	0.00124	0.00265
31	0.00783	0.00205	0.00050	0.00106	0.00254
34	0.00797	0.00188	0.00052	0.00047	
35	0.00865	0.00077	0.00055	0.00079	

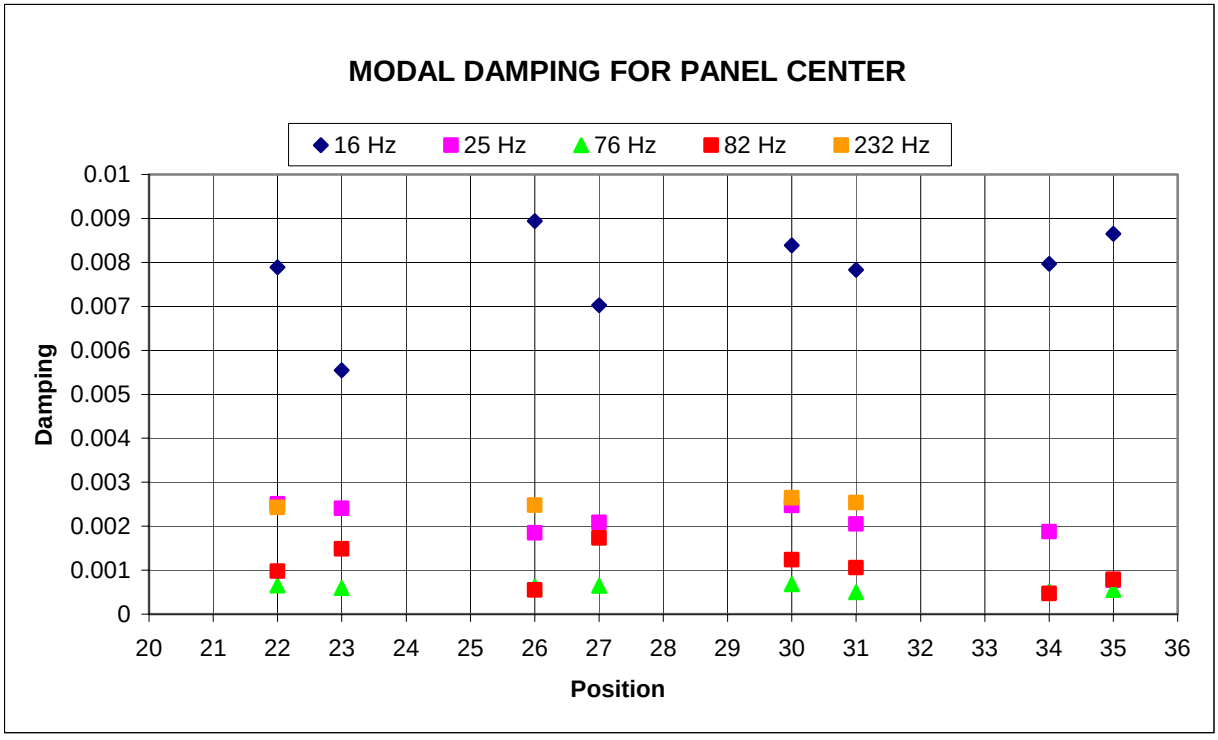

Figure 4.30 Modal Damping Values for Panel Center

Figure 4.30 shows again that the damping values for lower frequencies are higher and have more variation that the damping at higher frequencies. Figure 4.30 also shows that the position vertically or horizontally at which the damping values are measured has little impact on the damping.

The Rayleigh damping coefficients as well as the least fit curves of the damping values are shown in the following table and plots.

Table 4.7 Rayleigh Damping Coefficients for Panel Center

Position	α	β
22	0.76415	5.042E-06
23	0.82174	2.778E-06
26	0.93907	4.913E-06
27	0.47627	3.784E-06
30	1.56177	3.422E-06
31	1.31436	2.902E-06
34	0.76510	4.903E-06
35	0.78859	2.555E-06

For the center of the panel, the α coefficients have mean value of 0.929 and a standard deviation of 0.346, the β coefficients have a mean value of 3.787E-6 and a standard deviation of 1.038E-6.

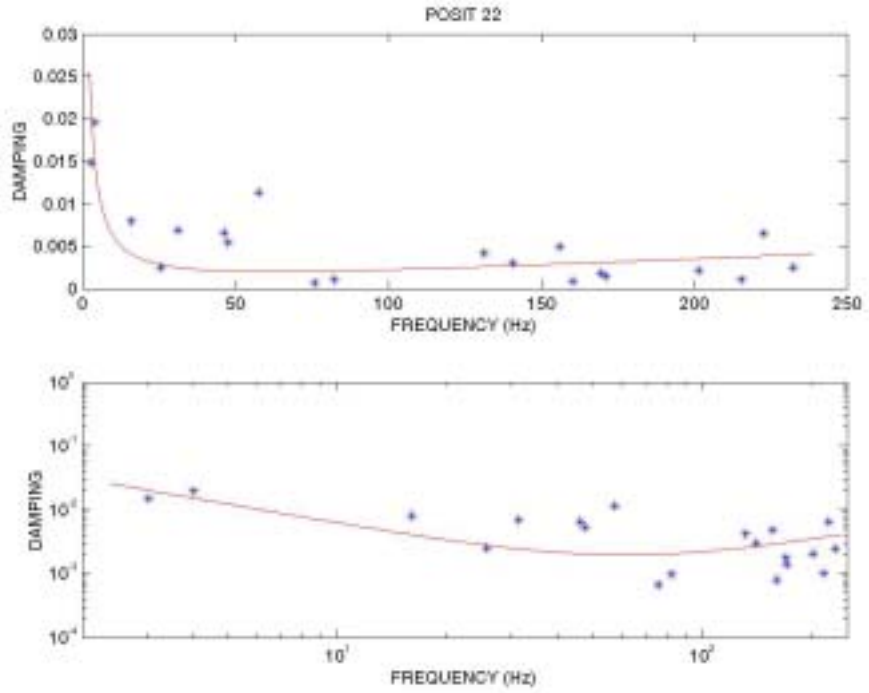

Figure 4.31 Best Fit & Rayleigh Damping Curves for Bulkhead Position 22

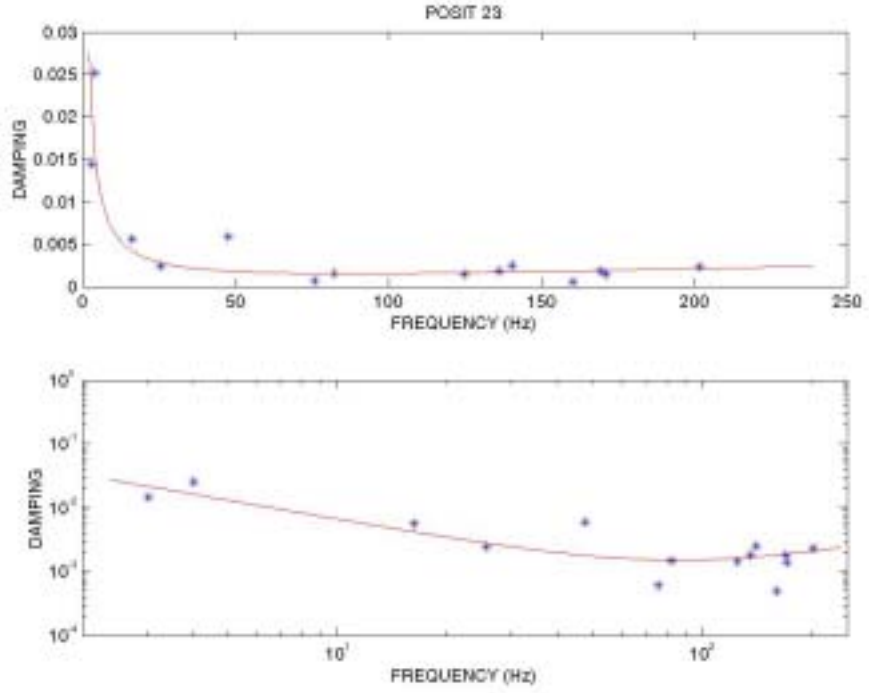

Figure 4.32 Best Fit & Rayleigh Damping Curves for Bulkhead Position 23

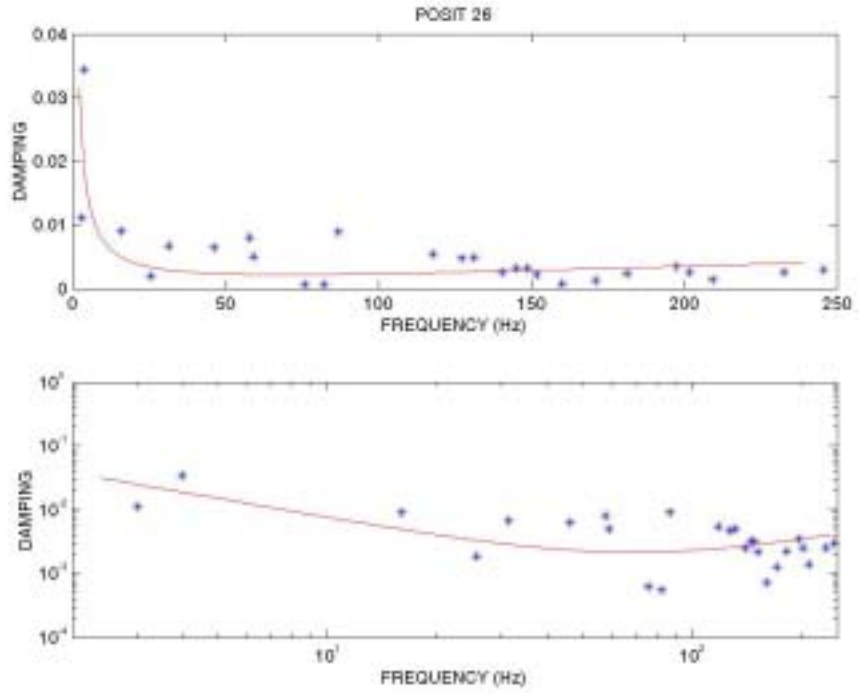

Figure 4.33 Best Fit & Rayleigh Damping Curves for Bulkhead Position 26

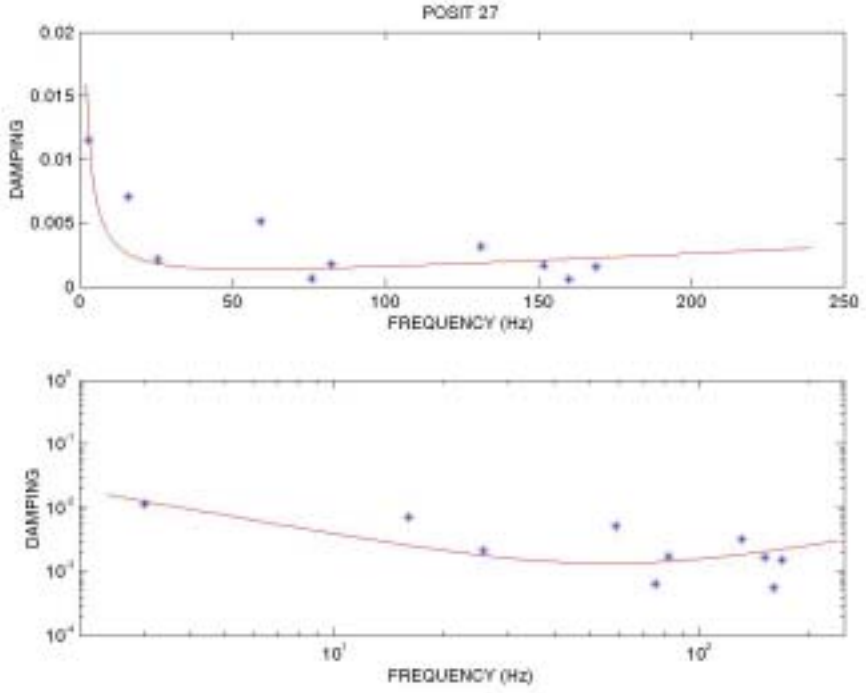

Figure 4.34 Best Fit & Rayleigh Damping Curves for Bulkhead Position 27

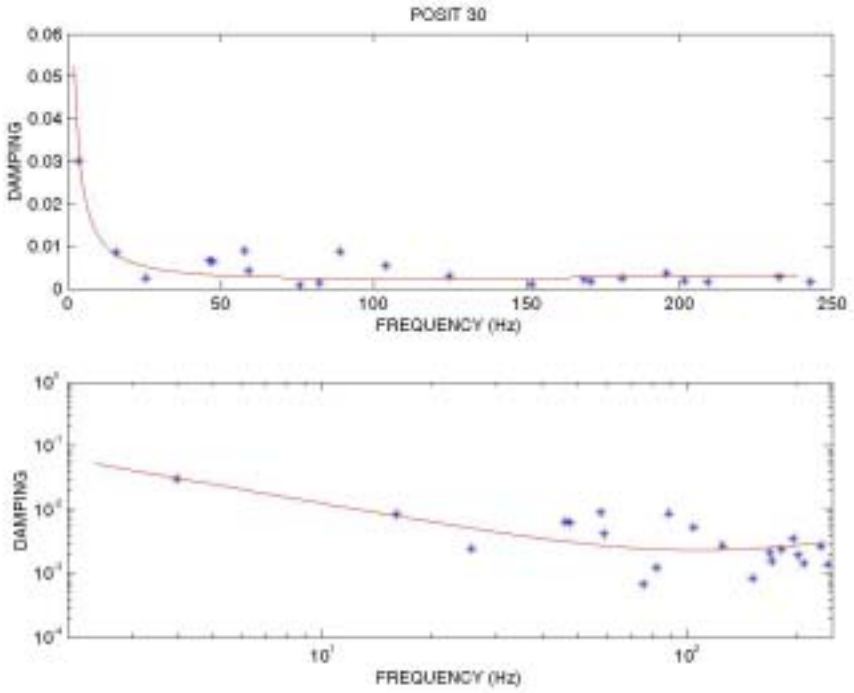

Figure 4.35 Best Fit & Rayleigh Damping Curves for Bulkhead Position 30

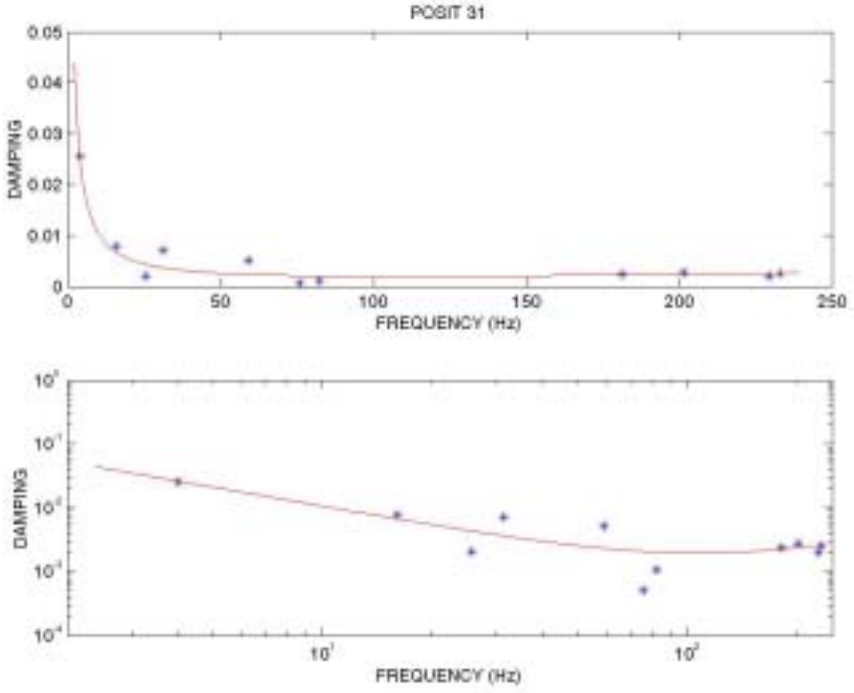

Figure 4.36 Best Fit & Rayleigh Damping Curves for Bulkhead Position 31

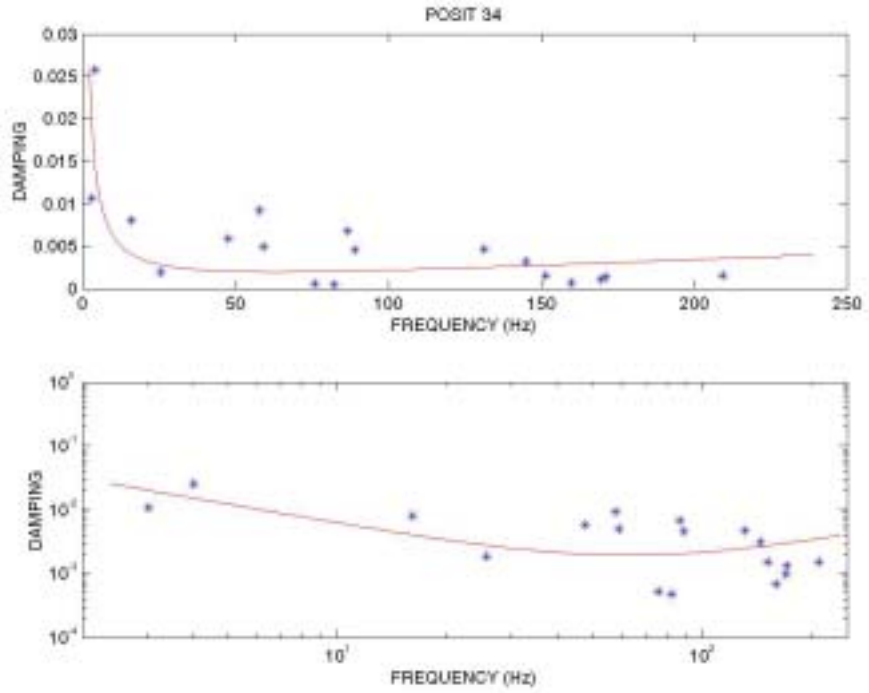

Figure 4.37 Best Fit & Rayleigh Damping Curves for Bulkhead Position 34

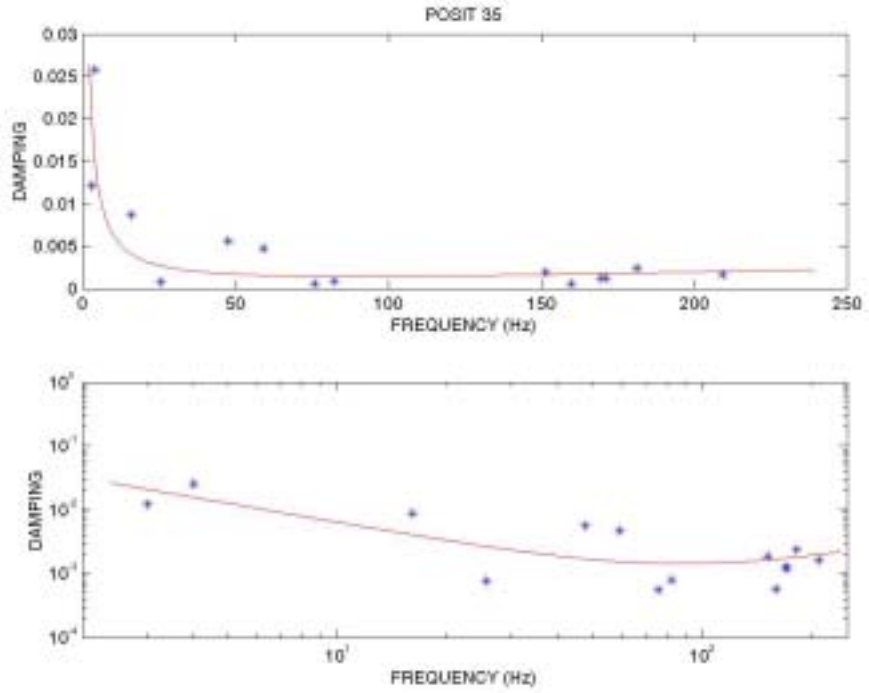

Figure 4.38 Best Fit & Rayleigh Damping Curves for Bulkhead Position 35

d. Damping for Unwelded Panel

As a baseline, the damping values in an unstiffened and unwelded panel were also calculated in the same manner as the watertight bulkhead. The measurements were taken from the positions indicated in Figure 4.12.

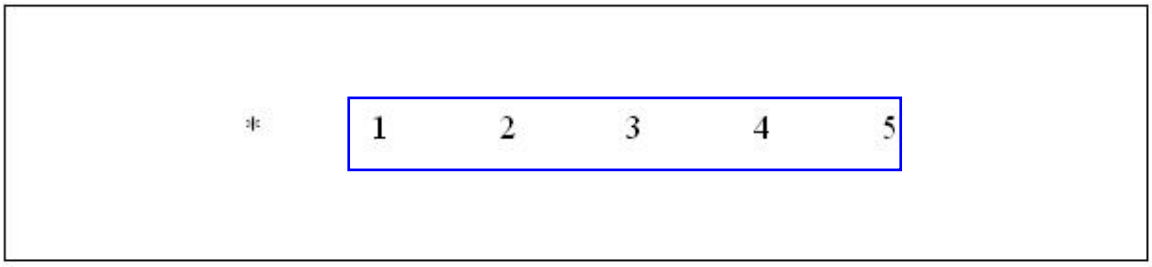

Figure 4.39 Measurement Locations for Unwelded Panel

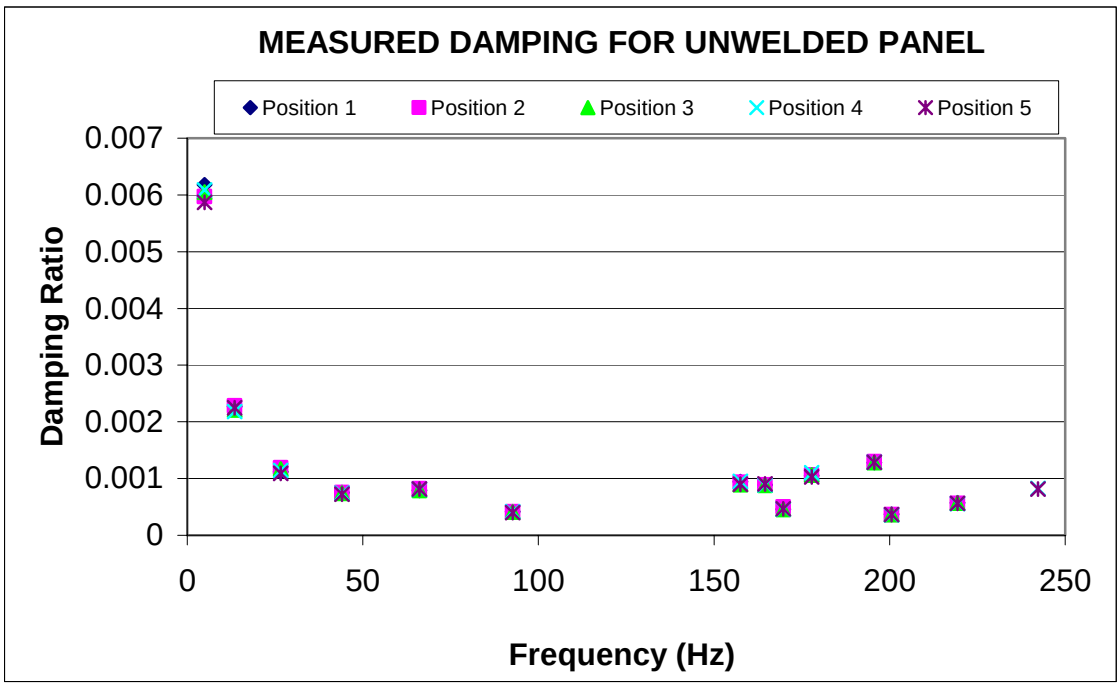

Figure 4.40 Measured Damping Values for Unwelded Panel

The damping trend in the unwelded panel follows the same decay trend as seen in the watertight bulkhead although the damping values are considerably less than those in the watertight bulkhead. It can also be seen that the damping values change very little in relation to the position on the panel.

Table 4.8 Damping at Modal Frequencies for Unwelded Panel

Position	Damping Values at Modal Frequencies						
	13 Hz	27 Hz	66 Hz	93 Hz	178 Hz	196 Hz	219 Hz
1	0.00227	0.00112	7.94E-04	4.14E-04	0.00105	0.00128	5.71E-04
2	0.00228	0.00119	8.23E-04	4.14E-04	0.00106	0.0013	5.61E-04
3	0.00221	0.00117	7.90E-04	4.13E-04	0.00106	0.00128	5.68E-04
4	0.00218	0.00114	8.08E-04	4.19E-04	0.0011	0.00129	5.57E-04
5	0.00225	0.00109	8.13E-04	3.99E-04	0.00103	0.00129	5.63E-04

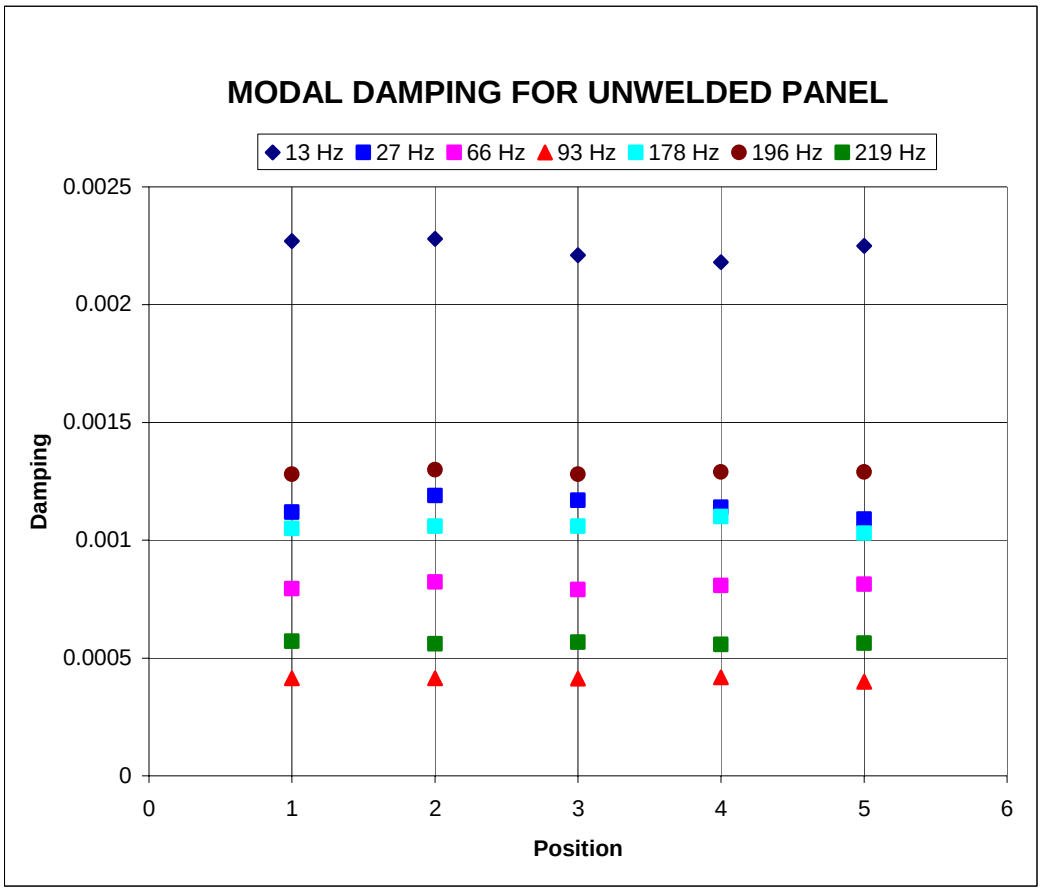

Figure 4.41 Modal Damping Values for Unwelded Panel

Just as in the watertight bulkhead, the lower frequencies produced higher damping values at each location as well as greater variation in the damping values, but still less variation than in the watertight bulkhead.

The Rayleigh damping coefficients are given in the following table. As can be seen the α and β coefficients for the flat panel are considerably less than the

damping in the watertight bulkhead which is also evident in the smaller damping values shown in Figure 4.40.

Table 4.9 Rayleigh Damping Coefficients for Unwelded Panel

Position	α	β
1	0.37970	1.04E-06
2	0.36943	1.07E-06
3	0.37198	1.04E-06
4	0.37341	1.03E-06
5	0.36276	1.02E-06

For the unwelded panel, the α coefficients have mean value 0.371 of and a standard deviation of 0.006. The β coefficients have a mean value of 1.039E-6 and a standard deviation of 1.645E-8. The mean values for both the α and β coefficients are significantly less than the mean values for any section of the watertight bulkhead which suggests that the watertight bulkhead overall has greater damping abilities than the unwelded panel.

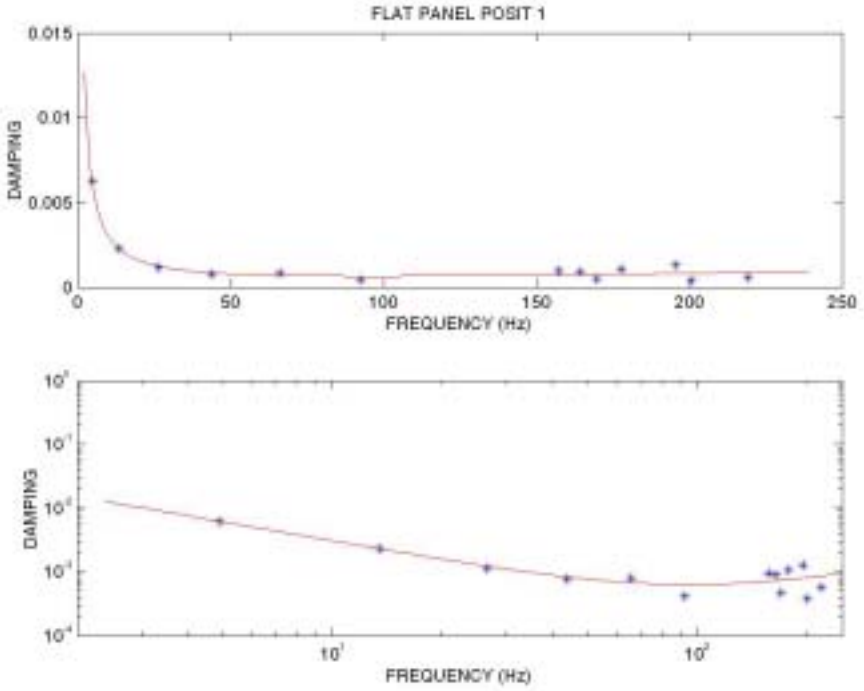

Figure 4.42 Best Fit & Rayleigh Damping Curves for Unwelded Panel Position 1

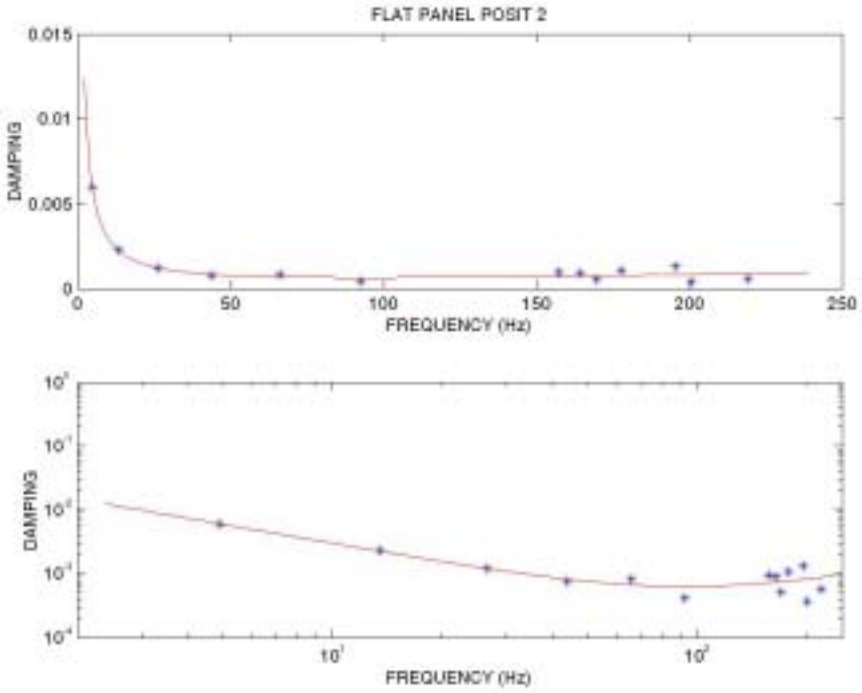

Figure 4.43 Best Fit & Rayleigh Damping Curves for Unwelded Panel Position 2

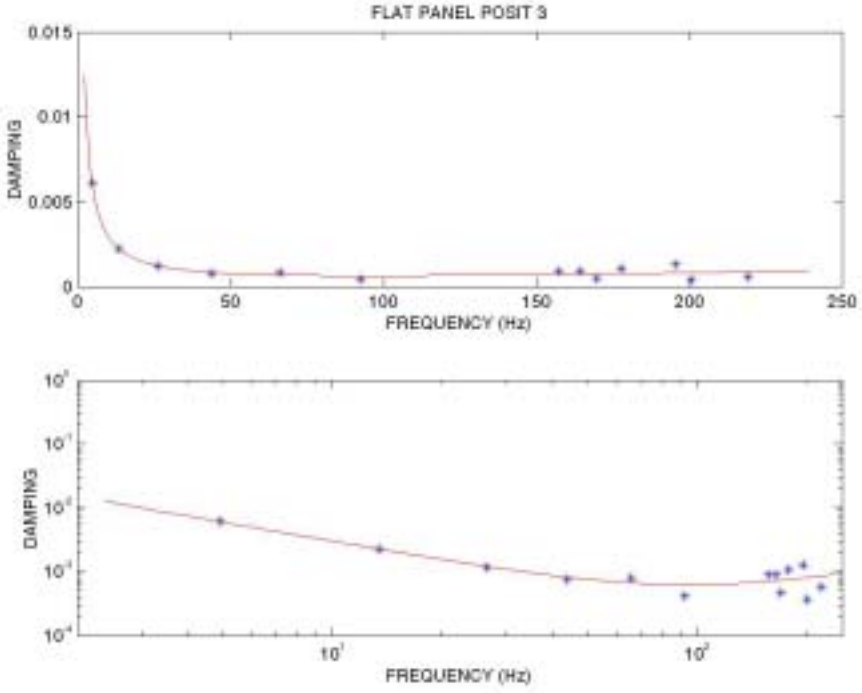

Figure 4.44 Best Fit & Rayleigh Damping Curves for Unwelded Panel Position 3

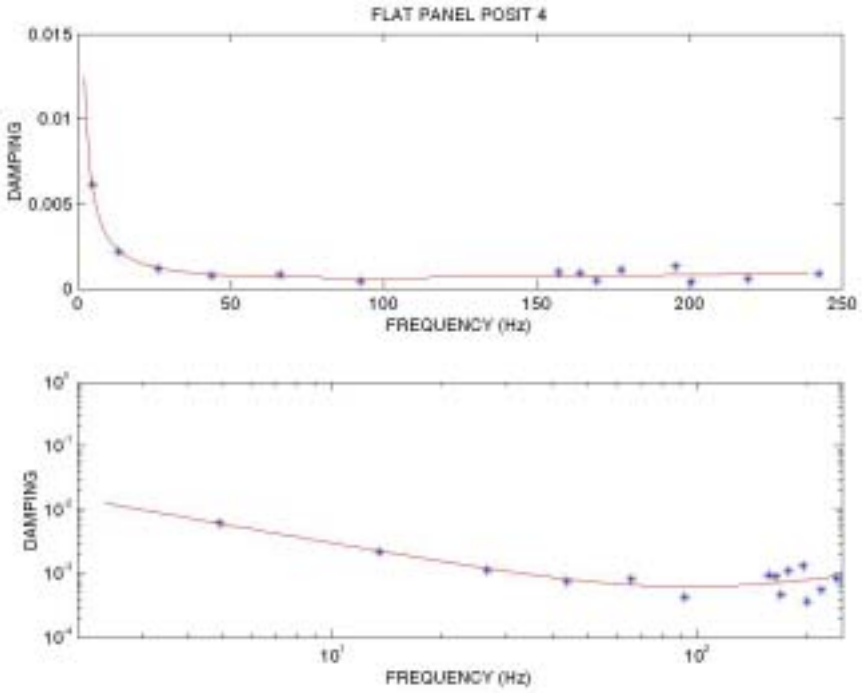

Figure 4.45 Best Fit & Rayleigh Damping Curves for Unwelded Panel Position 4

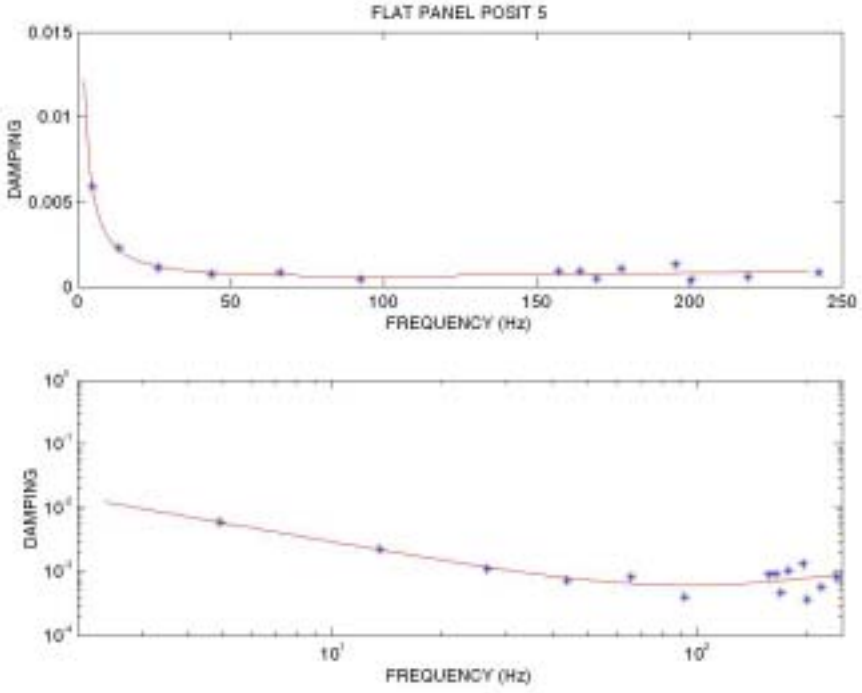

Figure 4.46 Best Fit & Rayleigh Damping Curves for Unwelded Panel Position 5

C. FINITE ELEMENT MODEL

The finite element model created in MSC Patran/Nastran was used to calculate the modal frequencies and mode shapes of both the watertight bulkhead and the unwelded panel.

Table 4.10 Modal Frequencies of Watertight Bulkhead FEM Model

Mode	Frequency (Hz)	Mode	Frequency (Hz)	Mode	Frequency (Hz)
1	2.9332	21	121.38	41	194.26
2	20.16	22	122.99	42	194.51
3	32.799	23	124.49	43	197.85
4	42.726	24	127.68	44	199.6
5	5.327	25	130.85	45	204.86
6	61.175	26	131.16	46	204.88
7	65.058	27	132.65	47	205.07
8	68.158	28	138.34	48	205.43
9	76.836	29	151.17	49	206.15
10	87.557	30	151.23	50	214.44
11	87.925	31	153.33	51	221.85
12	88.139	32	153.52	52	232.51
13	89.263	33	158.98	53	239.11
14	97.409	34	161.62	54	241.16
15	100.54	35	164.91	55	246.39
16	108.96	36	166.01	56	248.51
17	113.62	37	177.65	57	248.57
18	114.73	38	179.56	58	249.3
19	115.31	39	179.88		
20	116.91	40	190.86		

Table 4.11 Modal Frequencies of Unwelded Panel FEM Model

Mode	Frequency (Hz)	Mode	Frequency (Hz)
1	4.913	13	124.250
2	13.596	14	152.840
3	16.821	15	158.160
4	26.772	16	164.400
5	34.338	17	169.770
6	44.436	18	178.290
7	53.200	19	185.940
8	66.603	20	196.430
9	73.988	21	201.410
10	93.247	22	219.410
11	97.220	23	222.930
12	123.380	24	243.220

A comparison of the modal frequencies generated by the FEM model of the unwelded panel and the modal frequencies found using the experimental techniques

shows that the FEM model frequencies closely match those extracted using the experimental techniques, proving the veracity of the FEM model.

Table 4.12 Comparison of FEM and Experimental Modal Frequencies

Mode	FEM Frequency (Hz)	Experimental Frequency (Hz)
1	4.913	4.920
2	13.596	13.450
4	26.772	26.550
6	44.436	44.070
8	66.603	66.130
10	93.247	92.710
15	158.160	157.480
16	164.400	164.490
17	169.770	169.670
18	178.290	177.830
20	196.430	195.620
21	201.410	200.550
22	219.410	219.270
24	243.220	242.260

For the watertight bulkhead many of the highly resonant frequencies that were extracted from the experimental techniques were also present in the FEM model; however the FEM model also produced many more modes than were seen in the experiment which presents the possibility of the FEM model having generated false modes. Although the FEM models provide a good picture of the mode shapes and at what frequencies they occur, they do not provide information on the damping properties of the panels.

V. CONCLUSIONS & RECOMMENDATIONS

A. CONCLUSIONS

From the experiments performed in the course of this investigation it has become evident that the addition of welded stiffeners adds mass and stiffness to an otherwise flat panel and increases the Rayleigh damping coefficients, hence the overall damping of the structure. It has also been shown that the contribution of these welded stiffeners to increases in local damping values is relatively negligible. In other words the presence of a single weld or multiple welds between points on a structure did not significantly affect the level of damping at any point.

According to data recovered from the DDG-53 ship shock trials, the Rayleigh damping coefficients for ship structural damping were estimated as α=19.2 and β=2.09E-6. These experiments however yielded Rayleigh damping coefficients only as high as α=0.3797 and β=1.04E-6 for the unwelded panel and as high as α=1.562 and β=6.74E-6 for the watertight bulkhead. As a result of small increase in Rayleigh damping, particularly for the mass (α) coefficient between the unwelded panel and the watertight bulkhead and the large difference between the shock trial Rayleigh damping and the watertight bulkhead it is unlikely that the welds are a significant source of ship structural damping.

Further research into the field of ship structural damping is necessary and investigations should be made into the effects of painting, lagging, cable thru-ways, hatches, and other components that make up the structure of a ship.

THIS PAGE INTENTIONALLY LEFT BLANK

LIST OF REFERENCES

1. Shin, Y.S., "Damping Modeling Strategy for Naval Ship System", Report NPS-ME-03-003, Naval Postgraduate School, May 2003.

2. Betts, C. V., R. E. D. Bishop and W.G. Price, The Royal Institution of Naval Architects. 1976 "A Survey of Internal Hull Damping."

3. Harris, C.M., Shock and Vibration Handbook, 4TH Ed., McGraw-Hill Companies, 1996

4. Thomson, W.T. and M.D. Dahleh, Theory of Vibration With Applications, 5th Ed., Prentice-Hall Inc., 1998.

5. Ewins, D.J., Modal Testing: Theory and Practice, Research Studies Press Ltd., 1984.

THIS PAGE INTENTIONALLY LEFT BLANK

INITIAL DISTRIBUTION LIST

1. Defense Technical Information Center
   Ft. Belvoir, Virginia

2. Dudley Knox Library
   Naval Postgraduate School
   Monterey, California

3. Young S. Shin
   Naval Postgraduate School
   Monterey, California

4. Ilbae Ham
   Naval Postgraduate School
   Monterey, California

5. Fred Costanzo
   NSWC Carderock Division
   West Bethesda, MD

6. Gregory Harris
   NSWC Indian Head Division
   Indian Head, MD

7. Steve Rutgerson
   NSWC Carderock Division
   West Bethesda, MD

8. Jon Erskine
   Naval Postgraduate School
   Monterey, California